Master thesis

Stresses and deformation analysis of the storage system structure of the Ocean Grazer

By
Albert Altarriba i Subirana

Supervised By
prof. dr. A. Vakis

MSc Industrial Engineering

January 2020

Abstract

The global warming of the planet, mainly due to the excessive use of fossil fuels, and the consequences that are related to this phenomenon have implied a substantial increase in the bet on cleaner and more sustainable energy sources in the last decades. Ocean Grazer is a company created at the University of Groningen with the aim of developing technologies that make this transition possible. One of the elements on which it is carrying out research is an energy storage system, which aims to provide the electrical grid with energy coming from the wind and the ocean, with the ability to adapt at all times to the demand of the system.

The aim of this dissertation is to study the stresses and deformations that the structural part of the energy storage system, based on the suction anchoring technology, will have to endure during the installation stage. To this end, theoretical methods have been studied and used in order to find the boundary conditions of the system during the installation process; theories and methods of basic mechanics and materials resistance are backed by computer-assisted analytical calculations and simulations, which will be performed to verify the stability and resistance of the structure and, at the same time, optimize its design.

Contents

List of Figures

List of Tables

1 Introduction

1.1 The Ocean Grazer. Description of the system

The Ocean Grazer, a Dutch start-up founded in 2016, which has been developed within the University of Groningen (RuG) since 2014, is a versatile offshore renewable energy harvesting platform that integrates various subsystems, based in wave and wind power extraction as well as energy storage on site. The adaptable wave energy converter (WEC), the core of the technology, consists of a floater blanket on the ocean surface that adapts to the incoming wave features, allowing this novel technology, combined with an internal pumping system, to increase the power that can be extracted from the sea waves. Another of the subsystems is the Ocean Battery, an on-site loss-less energy storage system, able to control the energy output and adapt to the necessities of the electricity grid.
The first concept was based in a large scale wave energy converter designed to be implemented in deep waters like the Atlantic, where most of the ocean power resources worldwide can be found, meaning a greater impact to society. However, in terms of business approach, the current Ocean Grazer version will be implemented in shallower waters, such as the North Sea, with the aim of releasing these different subsystems so that various configurations and combinations of wind and wave harvesting as well as energy-storage are allowed.

2 Problem analysis

2.1 Problem context

The Ocean Grazer is an innovative project that works in a vast range of fields with the aim of defining the best solutions for its products, by adapting them to the new improvements developed throughout different iterative steps of the innovative process, carried out by researchers within the company. At the moment, the project remains within a laboratory stage, where these outputs are developed by means of conceptualization and materialization design, as well as prototyping. Design and subsequent optimization of models have been performed in order to define and understand the behaviour of the system while receiving inputs from the environment and how it will adapt to them in the best way, as well as how its output can be maximized and fulfil its expected functions.
To date, the storage system version is still being developed. In the process of designing a mechanical element or structure, a preliminary design is developed in the first stages in order to approach the problem in general terms, allowing the researchers to check the convenience of the chosen design parameters and get a first glimpse of the mechanics involved in that very first design. This paper, however, does not start from scratch; the Ocean Grazer company has already been working in a design. Some of the dimension parameters, which will be detailed later on in the requirements section, have been mainly determined by the power capacity of the system. However, some of its features have been defined based in literature and own experience in the field, since exhaustive research has not been previously carried out within the company, or it is investigated at the moment.
As in any company which intends to develop a product, one of the most relevant activities are those related to the performing of prototypes and testing. These can be virtual and physical representations with the aim of studying the shape, behaviour or its construction.

Table 1: *Tools for the development of products*

	Virtual	**Physical**
Shape	CAD model	Scale model
Behaviour	CAE model	Prototype
Construction	CAM model	Pre-series

The first step is the use of virtual representation tools, which contribute to the knowledge of the product. Different CAD models, with distinct levels of detail, have been implemented. For instance, see the one depicted in figure 3.
In order to validate the principle of functionality, preliminary prototyping has been carried out. On the one hand, a methacrylate structure of the whole module has been build so that the behaviour

of the flexible reservoir can be tested (see figure 1). A previous version of the storage system had the constraint of the bladder suffering a lot of wrinkles while moving. This test allowed to validate the improvements in the new design.
On the other hand, suction anchors testing is also implemented, by means of a methacrylate structure. The different processes involved in the installation of a suction anchor, as detailed later in the report, are tested (see figure 2).

Figure 1: *Prototype of bladder functionality*

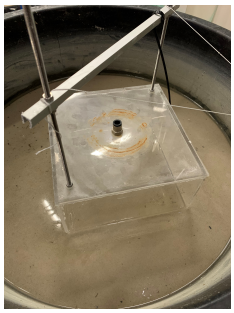

Figure 2: *Prototype of suction caisson functionality*

2.2 Problem definition

The Ocean Grazer team, with M van Rooij as chief technical officer (CTO) and principal problem owner, is interested in proving that the designs that are being developed for the Ocean Grazer storage system will have the expected performance.
Before moving forward in the development of the product, and therefore performing the indispensable testing in the last stages of the materialization design, simulation is a key step. From the point of view of time and cost resources, it is essential to simulate the product until the most reasonable and possible point.
As stated in the previous section, CAD designs and first-stages prototypes have been carried out, but no computer-aided engineering (CAE) simulations are available. In structural mechanics studies, finite element analysis (FEA) are of special interest to evaluate the stresses occurring within the element of study under certain boundary conditions.

3 System definition

This section aims to give a description of the system in order to define the boundaries of the problem analysed in this report. Based in the problem previously depicted, it is necessary to delimit the system that will be studied, that is the elements that will be taken into account and those which are out of the scope or unattainable so they will be excluded or will be considered as external actors.

3.1 System context

The Ocean Battery, the energy storage system, consists of a rigid tank at atmospheric pressure and a flexible reservoir - the bladder reservoir. When energy production exceeds the demand, the internal working fluid (assumed to be water in this paper) will be pushed from the rigid reservoir to the flexible one, this is inflating the bladder, so that the absorbed energy can be accumulated as potential energy; its deflation by means of the hydrostatic pressure of the ocean, allows the working fluid to go through a turbine, where the stored potential energy will be transformed into mechanical energy, and thereafter into electricity production, when it is needed. This structure will be attached to the seabed by means of suction anchoring, a well-known technology that allows the storage subsystem to be an independent module that, as specified in section 1.1, is meant to be combined with the other Ocean Grazer applications, but can also be used in currently working harvesting plants (i.e. offshore wind farms), storing the production of electricity but also as a mooring system (i.e. floating wind turbines).
Moreover, with the objective of making the most of the product in terms of versatility and possible

applications, the problem owners want the suction anchor design to work as an independent anchoring system; thus, the OG storage system could be placed on it, but also, any other structure. The proper definition of each specific case will be done in due course.

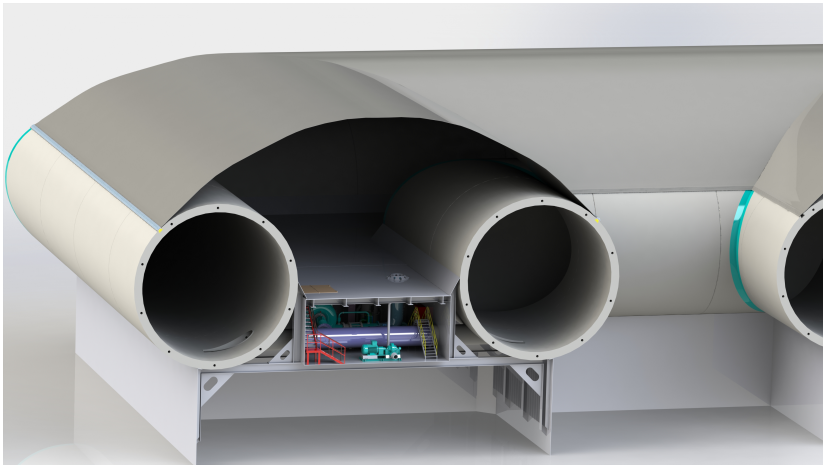

Figure 3: *Ocean Grazer storage system conceptual design. Module's section (Ocean Grazer B.V.)*

The structure is based in a module intended to allow for different configurations of the storage system itself, by means of attaching several modules to each other. These modules basically include, among many other structural and functional elements, the steel suction anchor, the rigid tanks made of concrete, and the flexible bladder made of EPDM synthetic rubber.
Unlike most of the cases found in literature, and as it will be detailed later on the following sections, the first design approach for the Ocean Grazer's suction caisson is in a rectangular shape with its skirts made of steel, over which the concrete pipes will be attached. They will include some internal plates and other structural elements in order to provide strength and stiffness to this vast structure, especially during the installation, to prevent them from bending or buckling. The reasons to conduct research into a new design of the suction caissons to those implemented until now are in part economical; thus, instead of cylindrical buckets, we can take advantage of the storage system layout to convert its bottom profile into the actual anchoring system. Therefore, the skirt of these caissons will be the base of each module.

Although the scope of this paper is to develop the design in function of the results obtained through the simulation analysis, there are several requirements (geometric specifications, materials, etc.) that the design has to meet in order to accomplish its functionality notwithstanding its viability in terms of constructive feasibility and economical profitability. These last issues are out of the scope of this project, but they are not neglected, so the decisions are taken with those stakeholders involved. The skirt of the suction caissons dimensions are 20 meters both width and deep, with a thickness of 3cm. The height of the skirt is initially set to 7m. The rigid tanks will have a cylindrical shape and will be made of concrete with fiber reinforcement. The outer diameter is set to 10m with a thickness of 0.5m.
As said above, the design is though to be done in modules to allow for different configurations; however, the Ocean Grazer is working in a layout based in 8 suction anchors attached to each other, as it is depicted in figure 4, of which 4 have a corner design. With the dimensions previously mentioned, this whole framework has a length and width of 70m at the concrete pipes level. The fact of having not only a suction caisson, but 8 of them, makes the installation process more controllable, allowing the structure to penetrate as desired by applying different suction pressures in each compartment.

3.2 Research boundaries

The system that is taken into consideration in this project is basically the steel suction anchors. The concrete pipes, as well as elements of union between each other, or with other elements are out of the scope.

The flexible bladder will not be of concern in this project because it is considered that, whether

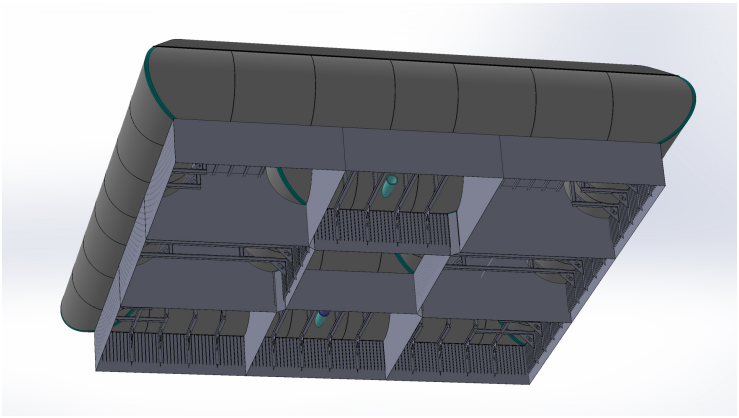

Figure 4: *Ocean Grazer storage system conceptual design. Overall layout seen from below (Ocean Grazer B.V.)*

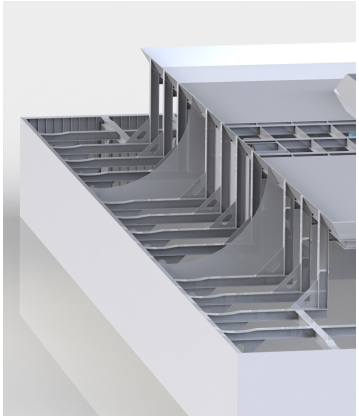

Figure 5: *Storage system steel structure (Ocean Grazer B.V.)*

the flexible reservoir is full or empty, the pressure applied to the outside of the bladder will be totally transmitted to the concrete and steel structures.

The contact between the steel skirts and the soil is known to be of high complexity. The interaction between both domains will depend, to a great extend, on the features of the terrain where it is installed. Certainly, there is a wide range of possibilities which are determined not only by the location, but also affected by the depth, leading to a series of layers of sand and clay with different physical properties. Related to it, phenomena of different nature can arise in the vicinity of the suction caisson, leading to a behaviour of challenging prediction. Therefore, the soil has been excluded from the simulation analysis, making the corresponding assumptions or simplifications in due time. Moreover, whenever necessary in analytical calculations, the soil properties used will be those of sand.
The interaction between seawater and the structure will also be simplified, and all forces and moments involved will be considered as external loads applied on the system. Other elements such as those related to the mooring system, installation or maintenance components will be out of the scope and their effect on the system will be treated with the same approach.

4 Scope of the thesis. Objectives

4.1 Research statement

Based on the previous sections, a goal statement is formulated to become the aim of this master thesis:

Study the mechanics of the Ocean Grazer's storage system in order to define the optimum design to fulfill its functions.

4.2 Objectives

Therefore, the research goals can be summarized as follows:

- Analytical study of the structure, taking into account the boundary conditions and the loading capacities, in order to verify the preliminary design, currently being designed by Ocean Grazer.
- Construction of a model to simulate the internal stresses and deformations that will occur within the main base structure, due to different forces that will be applied on it.
- Contribution to the actual design, by usage of this model, in terms of mechanical performance under the expected solicitations, and delivery of design guidelines.

4.3 Stages of study

During the structure's period of use in service, different stages will occur. This includes its transportation from the coastline to the offshore location where it is intended to be installed; the installation of the platform will imply the structure to be submerged until it reaches the seafloor, where a first penetration will proceed due to self-weight, followed by a suction penetration that will allow the system to be in full operation. Finally, another important stage is the future extraction of the structure, so that maintenance tasks can be done on the sea surface.

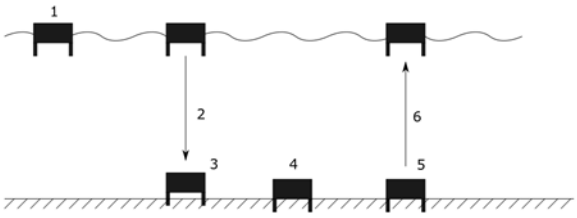

Figure 6: *Stages of suction caisson lifetime (Drawing done with Inkscape version 0.92).*

1. Transportation of the platform to the installation area.
   In this case, the solicitations that will outstand in comparison to other stages are the dragging forces and consequently, the resistance against its movement that the sea water will introduce. The impact of the waves should also be taken into consideration. Therefore, due to the importance of the interface between a solid and a fluid, a combination of structural mechanics and fluid dynamics would apply in this simulation case.

2. Installation.

3. Self weight penetration.
   The penetration of suction caissons into the seafloor is a process highly studied, and a lot of research on the matter can be found within the literature. If some simplifications are applied to the model, the penetration can be studied as a structural mechanics problem with a proper definition of the boundary conditions and the external loads acting on the system.

4. Anchoring with underpressure.
   Idem to the previous case.

5. Operational stages.
   Unlikely the suction caissons penetration and, as a matter of fact, the overall structure installation, in which the process is highly controlled, the structure is expected to suffer all kind of loads that can imply reaction forces and moments. Different situations depending on the rigid tanks state can apply:

   - Both tanks full with water
   - Both tanks half empty
   - Both tanks empty
   - Empty tank and full tank

6. Extraction for maintenance.

As previously discussed, it is still uncertain where the Ocean Grazer will be located or if there will be several versions that will make the product available for a range of different situations. The ultimate aim of the company is the Atlantic Ocean as the most favourable location, where a major depth will mean a higher hydrostatic pressure on the bladder, and thereafter a greater difference pressure between this flexible reservoir and the rigid one, allowing the system to store more potential energy. Although increasing depth will also affect the structure in terms of more extreme solicitations, which is of the interest of this thesis, only a scenario of 50m depth will be analysed in this report, which would apply for the North Sea.

As it will be seen later, while the sizing of the suction caisson, i.e. the skirt length and width,

has an influence on the holding capacity, the integrity of the structure will depend on the different extreme solicitations that will be applied on it.
It is easy to see that one of the most extreme cases will be during the suction assisted penetration within the installation process, when there will be a pressure difference between the inside and the outside of the caisson. This is the case that this thesis will study and analyse.

4.4 Research methodology. Outline for the thesis

In this section, the ways in which the author approached the purpose of exploring the mechanics of the structure, and indeed the convenience of the design, is described.
The analysis carried out can be divided into two types:

- Analytical calculations by means of a theoretical framework: on one hand, calculations based in methods found in literature related to suction caisson installation procedures that proved to have a high degree of accuracy and that, therefore have been accepted and used by different authors; on the other hand, the application of different basic mathematical theories related to resistance of materials and structural studies, in bases of verifying the results obtained by the simulation analysis, mentioned in the next point.
- FE analysis using Comsol Multiphysics version 5.4. A series of simulation tests will be carried out, starting from basic designs, and subsequently increasing its level of detail and complexity. A Comsol model will be built in order to obtain the desired results while changing different parameters of interest in terms of boundary conditions and geometric variables.

5 Literature research

5.1 Anchoring classification

The anchoring system of most offshore structures can be classified in one of these types:

- Surface gravity anchors or gravity-based structures (GBS): they are very large support structures that sit on the seabed, being hold in place by gravity, and resisting sliding and overturning loads by friction and soil bearing capacity.
- Drag anchors: consisting of a shank and a fluke. When the anchor is dragged, the fluke digs into the soil, creating a large holding capacity against horizontal loads.
- Driven piles: cylindrical and hollow steel pipes with a large lengthe to diameter (L/D) ratio, which are drilled or driven into the seabed. Their holding capacity relies on the friction between the pile length and the soil.
- Suction anchors or suction caissons

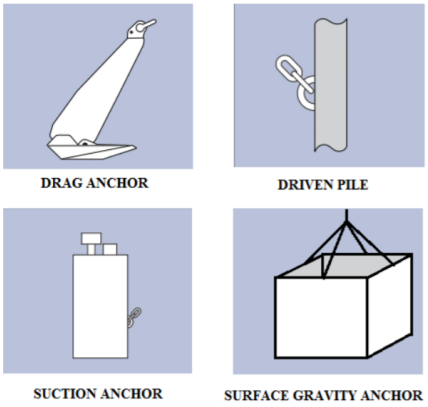

Figure 7: *Anchoring classification (Pollestad (2015))*

5.1.1 Foundations for Wind Turbine Generators

Wind turbine generators (WTG) can be supported on various types of foundations, which are shown in figure 8, and that are based on the 4 main typologies that haven been previously depicted. Figure 8 (a) shows a gravity base foundation, while (b), (d), (e) and (f) are different implementations of driven piles; (c) and (h) use suction caissons and type (g) is an example of drag anchors (Bhattacharya et al. (2017)).
As it will be explained in the next section, suction anchors have been used and combined with other technologies, so other possibilities can be also explored. For instance, tension leg platforms[1] can be anchored by driven piles (figure 8 (f)), but also with suction caissons.

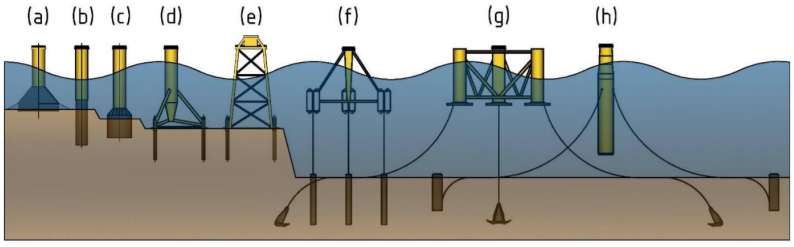

Figure 8: *Common types of foundations used to support WTGs; (a)Gravity-base (b)Monopile (c) Suction caisson (d)Tripod substructure supported by three driven piles (e)Jacket substructure supported by four driven piles (f)Tension leg platform (TLP) anchored to three driven piles (g)Drag anchors (h) Ballast-stabilised floating spar platform anchored to three suction caissons (Bhattacharya et al. (2017))*

[1]Tension leg platforms (TLP) is a concept which relies on steel cables tensioning a buoyant hull to the seafloor piling system

5.2 Suction caissons

Suction caissons are a relatively new form of offshore foundation usually based on large, cylindrical structures, mainly made of steel, closed at the top and open at the base such as the shape of an upturned bucket. Their principal applications are as a shallow foundation or as an anchoring system for all kind of designs, including floating structures, in which case the use of suction caissons has been increasing in recent years for many reasons; for instance, they are easier to install than impact-driven piles and can be used in deep water, as well as providing higher load capacities than for example, drag embedment anchors; another relevant characteristic is the fact that it can be rapidly removed by reversing the installation process, applying an overpressure inside the caisson cavity (Tassoulas et al. (2005)).
One main design challenge for this kind of structures is to penetrate the skirt deep enough to obtain the required capacity. That is why they are initially penetrated into the sea-bottom sediments under their own weight, and afterwards pushed to the required depth, applying a differential pressure inside the cavity by means of pumping water out of the interior. A factor which affects the penetration of the suction anchoring is the soil plug formed inside the caisson. When it is penetrated, soil will move through the open ended rib into the hollow caisson and form soil plug, which adds a resistive force against penetration (Guo and Chu (2014)).

Suction caissons have been used extensively since mid 1990's for anchoring purposes. For a long time they were known as suction anchors due to its installation technique—suction-installed; however, experience supports the idea that suction is remarkably important for the holding capacity of these foundations during their operational stage. If the structure is totally sealed, suction appears when loading is applied. While for soils with high permeability such as sand, this holding capacity can only be maintained for a short period of time, for low permeability soils like clays, this holding capacity can be maintained for years (Tjelta (2015)).

Table 2: *Typical size and skirt length L to diameter D ratio (L/D) values for different suction foundations applications (Tjelta (2015))*

Application	Typical diameter (m)
Moorings: $L/D < 5$	4-6
Subsea structures: $1 < L/D < 4$	5-10
Jackets: $L/D < 1$	8-15
Gravity base structures[2]: $L/D \ll 1$ *to* 1	23-35
Monopod tower	15-20

Tjelta (2015) gives typical values of size and L/D ratio recommended for different kind of suction foundations and its applications, depicted in table 2. The same source also explains the historic evolution of this technology, which is summarized in the following paragraphs.
The invention and implementation of suction caissons has slightly evolved from the first mooring tests by Shell in the late 1970's and its first commercial application at the Gorm field (North Sea, Denmark) in 1981, with twelve suction piles for the anchoring of an oil loading buoy.
During the 1990's suction foundations became a frequently used foundation, specially for the fact that offshore development moved to locations with deeper waters. The Snorre suction foundation (North Sea, Norway) in 1990-1992 was the first TLP foundation to use suction anchors. Also during this decade, the first two jackets which replaced pile foundations with suction caissons were installed for the Draupner "E" Riser Platform and the Sleipner "T" Processing Platform (North Sea, Norway).
From 2000, the high activity in deep waters exponentially increased the number of suction foundations used for offshore developments, and in the last decade, suction caissons have been considered for the renewable industry. With the objective of provididing practical support and encouraging the industry to use this technology, the Carbon Trust published the Offshore Wind Accelerator Suction Installed Caisson Foundation Design Guidelines. Suction caissons can be seen supporting the 8MW turbines at Vattenfall's European Offshore Deployment Centre in Scotland and Ørsted's Borkum Riffgrund 2 in Germany. (Cathie and Irvine (2019)).

[2]Although gravity-base structures are considered as another type of anchoring, some structures installed in poor ground conditions are founded on a system of suction caissons. In 1989, the Gullfaks C concrete platform was installed and meant the first time long concrete skirts acting as piles were implemented for a gravity-based structure. (Tjelta (2015))

6 Size verification of the suction caisson installed in sand

6.1 Introduction

A lot of research has been done and many analytical methods and formulations have been developed by different authors, to firstly approach the forces involved during the installation and usage of the system and predict other variables of interest, when designing the suction caissons, so that their integrity will not be compromised in any case. As previously said, this report does not aim to carry out a deep research on the optimization of the suction caisson for the Ocean Grazer in terms of the external conditions, but to build a model depending on them and predict the structure performance. However, the author considers that an estimation of certain parameters is of interest, so that the results obtained in this paper, and consequently, the decisions taken will better fit the reality and therefore will be closer to those implemented in future research. A verification of these theories is also out of the scope. All the theories used in the following sections are formulated by their authors for the case of a cylindrical caisson. The author of this thesis has adapted them into the case of a rectangular shape. Thus, the calculations conducted do not seek an exact output but an approximate order of magnitude of some parameters.

6.2 Holding capacity and sizing verification of the suction caissons

6.2.1 Loads estimation. The Ultimate Limit State

Due to the inflation and deflation of the flexible bladder, the rigid tanks will contain a certain portion of working fluid and the rest will be filled with air at atmospheric pressure. As any other solid submerged in water, it will appear a buoyancy force, that can be estimated as the volume of fluid displaced. In the particular case of the air cavity, the effect will be considerable since practically no weight will go against it. When all that fluid is pumped into the bladder, the rigid cylindrical reservoirs will be totally empty, leading to the most extreme situation. Its value is computed in the "Vertical load on the anchor" of table 3, along the vertical load due to mooring ($T_a \sin\theta_a$, see next paragraphs for explanation).

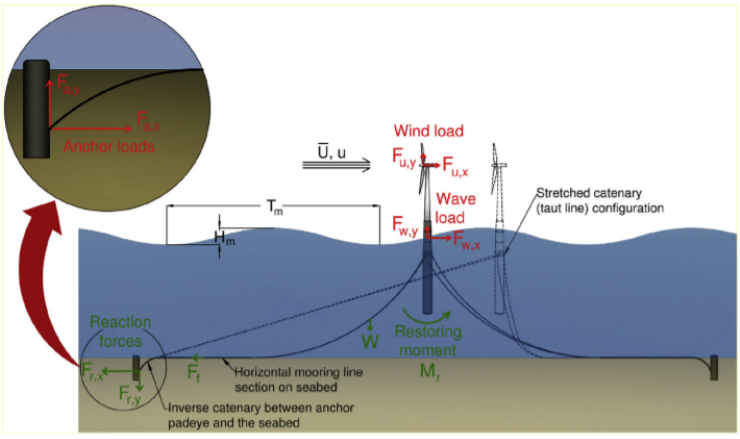

Figure 9: *Forces involved in offshore floating windmills anchored to suction caissons (Arany and Bhattacharya (2018))*

As exposed previously, the storage system is due to perform an additional functionality related to the anchoring of other renewable energy harvesting platforms, mainly Floating Offshore Wind Turbines (FOWT). Arany and Bhattacharya (2018) provides a simplified approach for finding an upper bound limit for the expected loads that a typical structure of this kind would transfer to the anchor through a catenary mooring.
The maximum load is assumed to be the sum of the wind load, drag and inertia components of the wave load, the wind drag on the structural components above water level and the current load on the floating platform.
Arany and Bhattacharya (2018) perform a series of calculations in order to obtain the ultimate limit state load for the Hywind floating platform, based in Scotland, which consists of five turbines

of 6 MW each. They conclude that the most extreme situation that the anchor will be subject to is the scenario with the combination of an extreme wave height (which happens every 50 years) and an extreme wind speed with the turbine shut down (also happens every 50 years), with a value of 23.1MN, applied through the mooring line. This force is applied totally horizontally to the embedded inverse catenary, located between the seabed and the anchor padeye, which is the device placed along the caisson skirt that provides an attachement point to the catenary.
As explained in previous sections, this paper does not aim to deeply look into an analytical study of a suction caisson, let alone a design that could fit in the requirements that a specific FOWT could demand. That is why the value of 23.1 MW applied through the catenary mooring (T_m in figure 10) is considered a good starting point in the suitability of the caisson design.

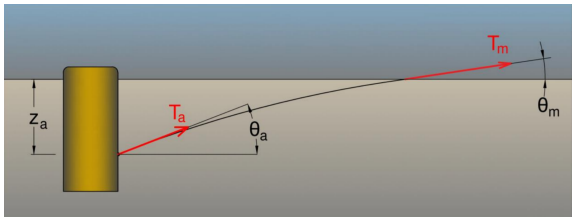

Figure 10: *Loads on the anchor lines (Arany and Bhattacharya (2018))*

The actual load applied on the suction caisson (T_a) is obtained by taking into consideration the load reduction on the inverse caternary from the mudline to the anchor padeye. The anchor padeye tension (T_a) and the angle (θ_a) can be obtained by solving:

$$\frac{T_a}{2}(\theta_a^2 - \theta_m^2) = z_a Q_{av} \tag{1}$$

$$\frac{T_m}{T_a} = e^{\mu(\theta_a - \theta_m)} \tag{2}$$

where

T_a	Tension at the anchor padeye
T_m	Tension at the mudline
θ_a	Angle of the tension at the anchor padeye to horizontal
θ_m	Angle of the tension at the mudline to horizontal
z_a	Depth of the anchor padeye below mudline
μ	Friction coefficient between the forerunner (chain, rope or wire) and the soil
Q_{av}	Average soil resistance between the mudline and the padeye.

For sand, the padeye depth (z_a) is related to the caisson's height by $z_a/L = 2/3$; in that case θ_m is considered null, so that the mooring line is transmitting a totally horizontal force T_m; a value of 0.25 is taken for the friction coefficient μ; the average soil resistance is calculated as:

$$Q_{av} = \frac{1}{2} A_b N_c \gamma' z_a \tag{3}$$

where

A_b	effective unit bearing area of the forerunner (according to Arany and Bhattacharya (2018) it equals the diameter of the rope or wire, and 2.5-2.6 times the bar diameter in case of using a chain; a value of 1.2 has been considered in these calculations)
N_c	bearing capacity factor (a value of 14 has been used)
γ'	submerged unit weight of the soil (a value of 8.5 kN/m^3 has been used)

6.2.2 Horizontal holding capacity of suction caissons in sand

When anchored in sand, the horizontal capacity of the caisson can be estimated (Chatzivasileiou (2014)) as follows

$$H_{c,sand} = LQ_{av} = \frac{1}{2} A_b N_q \gamma' L^2 \approx \frac{1}{2} D_o N_q \gamma' L^2 \tag{4}$$

where N_q is another bearing capacity factor, which can be obtained as

$$N_q = e^{\pi \tan \phi} \tan^2(45^o + \frac{\phi}{2}) \tag{5}$$

where ϕ is the internal angle of friction of the soil, an intrinsic parameter of the sand where the caisson is anchored (in that case a value of 30º has been taken into account for ϕ). These and other parameters will be used again in the calculations of the suction caisson installation, in section 6.3 (detailed information about soil parameters has been summarized in appendix A.6).
In this case, since the design is not cylindrical but rectangular, the outer diameter D_o is approximated with the skirt width (that is $D_o = w_o = l_o = 20$ meters).

6.2.3 Vertical holding capacity of suction caissons in sand

Vertical holding capacity of a suction anchoring in sand when tensile load is applied very slowly can be calculated as a fully drained study (Houlsby et al. (2005)). That would be the case of concern, since the buoyancy forces, most responsible of the uplift load, change progressively during the storage system operational stage.
The resistance of the caisson is calculated as the sum of friction on the outside (Q_{out}) and the inside (Q_{in}) of the skirt. These forces are calculated as the shear stress acting on the skirt area of the caisson due to its contact with the soil. It is assumed that horizontal effective stress is a factor K times the vertical effective stress. Taking into account the mobilised angle of friction between the caisson wall and the soil (δ), then the shear stress is obtained as $\sigma_v^{'} K \tan \delta$.
The expression that Houlsby et al. (2005) propose is the following:

$$\begin{aligned} V_{c,sand} = \quad & W_{rt} + W_{sc} \\ & + \gamma^{'} Z_o^2 \left(exp\left(-\frac{h}{Z_o}\right) - 1 + \left(\frac{h}{Z_o}\right)\right) (K \tan \delta)_o P_o \\ & + \gamma^{'} Z_i^2 \left(exp\left(-\frac{h}{Z_i}\right) - 1 + \left(\frac{h}{Z_i}\right)\right) (K \tan \delta)_i P_i \end{aligned} \tag{6}$$

where

$V_{c,sand}$	vertical capacity in sand	(kN)
W_{rt}	Concrete rigid tank weight	(kN)
W_{sc}	Steel suction caisson weight	(kN)

Further detailed information of the obtaining of this formula and the significance of each parameter can be found in appendix A.

6.2.4 Case study

The holding capacity of suction caissons is normally determined in terms of an envelope which takes into account both horizontal and vertical load components applied on the anchor, as shown in the following expression (Arany and Bhattacharya (2018)):

$$FP = \left(\frac{H_u}{H_c}\right)^a + \left(\frac{V_u}{V_c}\right)^b < 1 \tag{7}$$

where

$a = \frac{L}{D_o} + 0.5$; $b = \frac{L}{3D_o} + 4.5$

In this paper, the simplification of considering the outer diameter D_o as the skirt width is assumed ($w_o = l_o = 20$ meters). L is the lenght of the caisson.
In equation 7, as explained before, H_c and V_c are the horizontal and vertical capacities respectively, whereas H_u and V_u are the applied loads. FP is the failure criterion so that its maximum value can be 1.

The required dimensions of the suction caisson necessary to anchor the storage system of the

Ocean Grazer as well as other floating platforms are calculated by applying the equations explained in the previous sections and using the parameters showed in the following table.
Regarding the method used to calculate the vertical holding capacity, its main limitation is the need to estimate many input parameters (mainly K, δ, ϕ and $\gamma^{'}$) from laboratory tests of the soil in which the caisson is intended to be installed. Therefore, estimates of these parameters are found based upon typical values that would imply the most unfavourable results (the values used have either been specified in the previous paragraphs or have been included in table 3).

Table 3: *Minimum caisson dimensions for various length to diameter ratios, installed in sand*

Length-to-width ratio of caisson	L/w_o	1,222	**0,259**	0,131
Caisson width [m]	w_o	10	**20**	30
Minimum required length [m]	L_{min}	12,22	**5,18**	3,93
Wall thickness [m]	t	0,02	**0,03**	0,05
Weigth of the caisson [kN]	$W_{rt} + W_{sc}$	7027	**14055**	21085
	$(K \tan)_o$	0,50	0,50	0,50
	$(K \tan)_i$	0,50	0,50	0,50
Max vertical capacity [kN]	V_c	28153	**44893**	68332
Max horizontal capacity [kN]	H_c	116782	**41968**	36236
Anchor padeye depth [m]	z_a	8,15	3,45	2,62
Angle at the padeye [deg]	θ_a	40,05	16,11	12,12
Tension at the padeye [kN]	T_a	19396	21532	21910
Vertical load on the anchor [kN]	$V_u = T_a \sin\theta_a$+buoyancy forces	27977	**37034**	51432
Horizontal load on the anchor [kN]	$H_u = T_a \cos\theta_a$	14847	**20686**	21422

Therefore, for the case of a 20m caisson width, the minimum required length turns out to be somewhat greater than 5m, so that the holding capacity of the anchor is enough. However, several assumptions and simplifications have been done, and the variation of soil parameters has certainly proved to change the results. Hence, the premise of a 7m skirt length is assumed.

6.3 Self-weight and suction assisted penetration

Once the overall geometry has been verified within the previous sections, this chapter turns the attention to the process of installing the structure by means of two stages: self-weight and suction assisted penetration. The aim of studying these processes is to calculate certain variables related to the installation of suction caissons that will be of concern to later simulation processes; among others, the self-weight penetration depth, the suction-assisted penetration depth, the suction applied inside the caisson or the suction limit that can be applied are elements of interest.
The basic equation for the installation calculations is as follows:

$$V^{'} + sA_i = Q_{in} + Q_{out} + Q_{tip} \tag{8}$$

where

- A_i Internal plan area of caisson (internal top plate area)
- Q Resistance force
- s Suction applied during the suction caisson installation (pressure outside caisson minus pressure inside caisson)
- $V^{'}$ Effective vertical load, taking into account any buoyancy effects

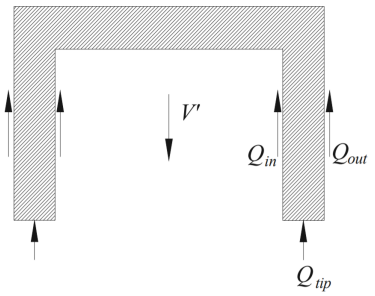

Figure 11: *Forces acting on suction caissons during the installation stage (Guo and Chu (2014))*

There are two main types of calculation methods in literature.

- Mechanism-based methods. They are based on using the geotechnical properties of the soil and mechanism-based calculations of the loads on the caisson
- Cone penetration test (CPT) based methods. They use empirical factors applied to CPT measurements to convert them to estimates of loads on the caisson.

According to Cathie and Irvine (2019), both approaches often lead to rather similar predictions. In this paper, only methods based in the first type will be presented and used to make the estimations. It is assumed that the penetration velocity is constant, and that the driving forces and soil resistance are balanced during the whole installation process.

6.3.1 Self-weight penetration

The self-weight penetration, which occurs in absence of suction, is a crucial part of the installation process that creates a seal at the edge of the foundation, allowing the later suction to take place. According to Houlsby and Byrne (2005), the resistance on the caisson can be calculated in a similar approach as done by Houlsby et al. (2005) to calculate the vertical holding capacity, explained in the previous sections; thus, as the sum of friction on outside and inside, an the end bearing on the annulus. In a similar way, the enhancement of vertical stress close to the pile due to frictional forces is taken into account. In the special case where m is taken as a constant, and uniform stress is assumed within the caisson, the following expression can be formulated to calculate the self-weight penetration depth:

$$\begin{aligned} V^{'} = {} & \gamma^{'} Z_o^2 \left(exp\left(\frac{h}{Z_o}\right) - 1 - \left(\frac{h}{Z_o}\right)\right)(K\tan\delta)_o(P_o) \\ & + \gamma^{'} Z_i^2 \left(exp\left(\frac{h}{Z_i}\right) - 1 - \left(\frac{h}{Z_i}\right)\right)(K\tan\delta)_i(P_i) \\ & + \sigma^{'}_{end}(A_{end}) \end{aligned} \tag{9}$$

where $\sigma^{'}_{end}$ can be calculated as:

$\sigma^{'}_{end} = \sigma^{'}_{vo} N_q + \gamma^{'}(t - \frac{2x^2}{t})N_\gamma$ where $x = \frac{t}{2} + \frac{(\sigma^{'}_{vo} - \sigma^{'}_{vi})N_q}{4\gamma^{'}N_\gamma}$ if $\sigma^{'}_{vo} - \sigma^{'}_{vi} < \frac{2tN_\gamma}{N_q}$

$\sigma^{'}_{end} = \sigma^{'}_{vo} N_q + \gamma^{'} t N_\gamma$ if $\sigma^{'}_{vo} - \sigma^{'}_{vi} \geqslant \frac{2tN_\gamma}{N_q}$

$\sigma^{'}_{vo}$ and $\sigma^{'}_{vi}$ can be obtained as follows:

$$\sigma^{'}_{v} = \gamma^{'} Z_i \left(exp\left(\frac{z}{Z_i}\right) - 1\right) \tag{10}$$

The author has checked if the results obtained with equation 9 are reliable, comparing them to real data, shown in examples by Houlsby et al. (2005). The assumption of a constant value of m=1.1 proves to be correct. The values of self-weight penetration depth will be presented in due course.

6.3.2 Suction-assisted penetration

The suction-assisted penetration is achieved by applying a suction s, that is the pressure with respect to the ambient seabed water pressure, so that the absolute pressure in the caisson would be $p_a + \gamma_w h_w - s$, where p_a, γ_w and h_w are the atmospheric pressure, the unit weight of water and the water depth respectively. Continuing with the reference of Houlsby and Byrne (2005), a formulation to calculate the suction applied, depending on the depth, can be done. In this case, this suction generates flow within the soil, where the pore pressure gradients are beneficial for the installation process and must be accounted for.
In the special case where we assume that the internal vertical effective stress is reduced sufficiently that the failure mechanism involves movement of soil entirely inwards, m is taken as a constant, and uniform stress is assumed within the caisson, the following expression can be formulated:

$$\begin{aligned} V^{'} + s(A_i) = {} & \left(\gamma^{'} + \frac{as}{h}\right) Z_o^2 \left(exp\left(\frac{h}{Z_o}\right) - 1 - \left(\frac{h}{Z_o}\right)\right)(K\tan\delta)_o(P_o) \\ & + \left(\gamma^{'} - \frac{(1-a)s}{h}\right) Z_i^2 \left(exp\left(\frac{h}{Z_i}\right) - 1 - \left(\frac{h}{Z_i}\right)\right)(K\tan\delta)_i(P_i) \\ & + \left(\left(\gamma^{'} - \frac{(1-a)s}{h}\right) Z_i \left(exp\left(\frac{h}{Z_i}\right) - 1\right) N_q + \gamma^{'} t N_\gamma \right)(A_{end}) \end{aligned} \tag{11}$$

The factor a accounts for the fraction of the suction transmitted to the caisson tip. It is a function of the caisson penetration and soil permeability, and can be obtained with the following expressions:

$$a = \frac{a_1 k_f}{(1 - a_1) + a_1 k_f} \tag{12}$$

where $a_1 = c_0 - c_1(1 - exp(-\frac{h}{c_2 D}))$; $c_0 = 0.45$; $c_1 = 0.36$; $c_2 = 0.48$; ; k_f is the ratio between the inside and the outside permeability (a value of 3 is assumed). The diameter D will be assimilated to the width and length of the caisson.
According to Houlsby and Byrne (2005), more complex variations can be considered but cannot be solved analytically. Hence, if equation 11 is used, the results vary significantly depending on the factor m. Comparing results obtained with equation 11 to real data, it has been found that a value of 1.5 is appropriate. Chatzivasileiou (2014) also concludes that using this value is a good assumption.

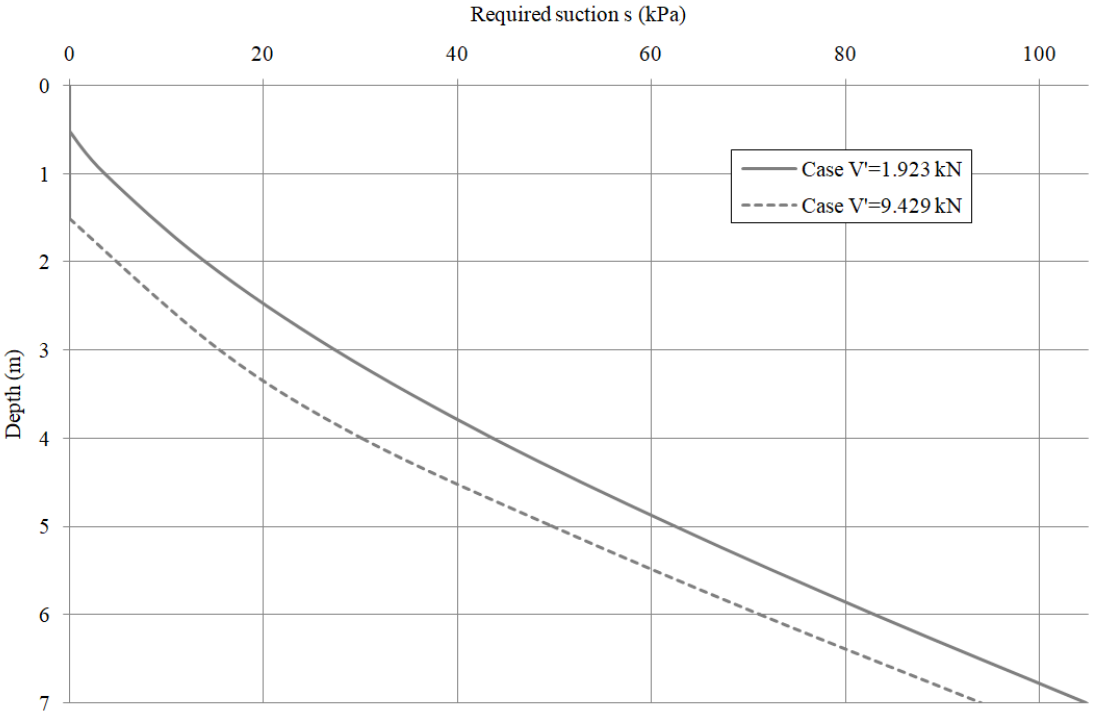

Figure 12: Calculated required suction using equations 9 and 11 for the cases of an effective weight with values of $V^{'} = 1923kN$ and $V^{'} = 9429kN$ respectively

In figure 12 two cases are depicted, in which the vertical effective weight is set to 1923kN and 9429kN respectively (data used in the following sections). The main limitation of applying equations 6.3.1 and 11 is the need of estimating many input parameters, most of them related to the soil. According to data provided by Houlsby and Byrne (2005), the most onerous soil conditions are used, so that the worst situation is estimated:

Table 4: *Parameter values used in the implementation of equations 9 and 11, depicted in figure 12*

Parameter	**Description**	**Value**	**Units**
$\gamma^{'}$	Submerged unit weight of the soil	8.5	kN/m^3
K$\tan\delta$	Relation between vertical and horizontal stress, and angle of friction between steel and soil	0.8	
Φ	Internal angle of friction of the soil	45	[degrees]
N_q	Bearing capacity factor (overburden)	134.9	
N_γ	Bearing capacity factor (self-weight)	262.7	
k_f	Ratio of permeability within caisson to outside caisson	3	

Critical suction

In sandy soils, the resistance that oppose the skirt's penetration is remarkably higher than that encountered in soft clay. That is why there is a need for reduction of the tip resistance, which is achieved by a seepage flow, generated by the pressure difference. This seepage flow is possible in high-permeable soils such as sand, and leads to a decrease of effective stresses around the skirt. However, failure during the suction assisted installation phase occurs when certain thresholds are exceeded. Basically, surpassing the critical suction may cause either formation of piping channels or cavitation of pore water. As proved by Ibsen and Thilsted (2010), the following expressions are accurate when looking for the critical suction when the installation is in sandy soils:

$$\frac{p_{crit}}{\gamma' D} = \frac{h}{D}\left(\frac{s}{h}\right) \tag{13}$$

where

p_{crit}	critical suction
γ'	submerged unit weight of soil
s	seepage length
h	penetrated length
D	suction caisson diameter

The following expression approximates $(\frac{s}{h})$ for the installation in homogeneous sand. Equivalent expressions have been formulated by other authors and lead to similar results.

$$\left(\frac{s}{h}\right)_{ref} = 2.86 - \arctan\left(4.1\left(\frac{h}{D}\right)^{0.8}\right)\left(\frac{\pi}{2.62}\right) \tag{14}$$

The following empirical expression is given to approximate $(\frac{s}{h})$ in case of having a layered sand, where L_Ω is the distance, from the seabed, to a flow boundary. It is assumed that the presence of silt layers act as impermeable flow boundaries and change the flow field around the skirt tip as it approaches the layer, increasing the suction threshold against piping.

$$\left(\frac{s}{h}\right) = \left(\frac{s}{h}\right)_{ref} + 0.1\left(\frac{D}{L_\Omega}\right)\left(\frac{h}{L_\Omega - h}\right)^{0.5} \tag{15}$$

Figure 13 shows the relation between the critical suction pressure and the penetration ratio, for both homogeneous and layered sand cases. On the one hand, it can be seen that a large ratio L_Ω/D means that the silt layer is deep, having little influence on the seepage flow, and therefore, it is assimilated to homogeneous sand. On the other hand, in layered sand cases, it gets to a point in the penetration ratio (h/D), in which the critical suction grows infinitely. This means that the effect of layers of silt is enough to prevent seepage flow to occur, and therefore there is no possibility of soil failure.

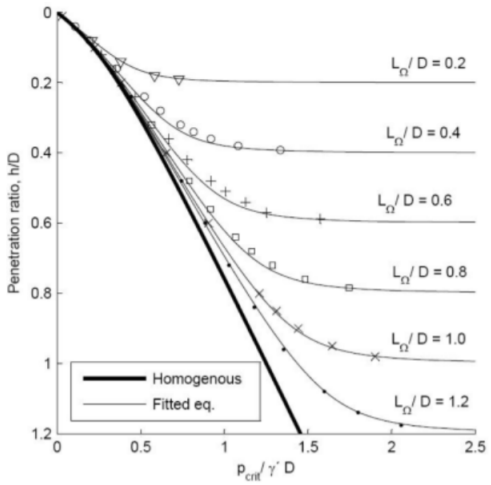

Figure 13: *Normalized critical suction versus relative penetration. Homogeneous sand and layered sand with different ratios L_Ω/D (Ibsen and Thilsted (2010))*

Ibsen and Thilsted (2010) compares these empirical curves to actual data obtained by three tests with different soils: homogeneous sand, sand with a silt layer further down the skirt tip, and sand with silt layers within the penetration depth. They get to the conclusion that a suction close to, or even higher than the critical suction for the homogeneous case, can be applied without significant consequences. Also, it is stated that the presence of thin silt layers will increase the suction thresholds against piping. However, their results also show that the expressions previously shown are a good estimate, at least as a first approach, to the suction needed to overcome the resistance during the installation of the buckets. Therefore, equations 13 and 14 are used to predict the suction that will be required to make the suction anchor to penetrate into the seabed and compare it to the results obtained with equation 11. The assumption of assimilating the system to a 20m diameter cylindrical caisson is made. ($\gamma^{'}$=8,5 is used)

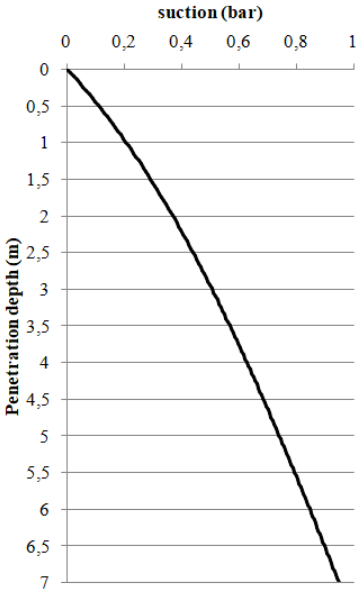

Figure 14: *Suction needed to penetrate a 20m diameter cylindrical suction caisson versus depth*

As it is depicted in figure 14, the more penetrated the suction caisson is, the more suction is needed. The maximum under-pressure ($\sim 1bar$) will be taken into account at anytime in the following chapters, as a conservative measure.

7 Suction caisson design

7.1 Theoretical background

In the following subsections, different theories and methodologies are depicted, which will be used later on.

7.1.1 Structural security

In mechanical resistance calculations, the safety factor is mainly applied in two ways:

- Multiplying the value of the solicitations or forces acting on a resistant element (E_m) by a coefficient greater than 1 (magnification factors). In this case, it is calculated as if the system was requested to a greater extent than actually expected (E_d).
- Dividing the favorable properties of the material that determine the design (R_m) by a number greater than 1 (reduction factors). In this case, the material is modeled as if it had worse properties than expected (R_d).

A structure is supposed to satisfy the ultimate limit state criterion if all factored (magnified) stresses (such as bending, shear, tensile or compressive) are below the factored (reduced) resistances calculated for the section under consideration:

$$E_d \leqslant R_d$$

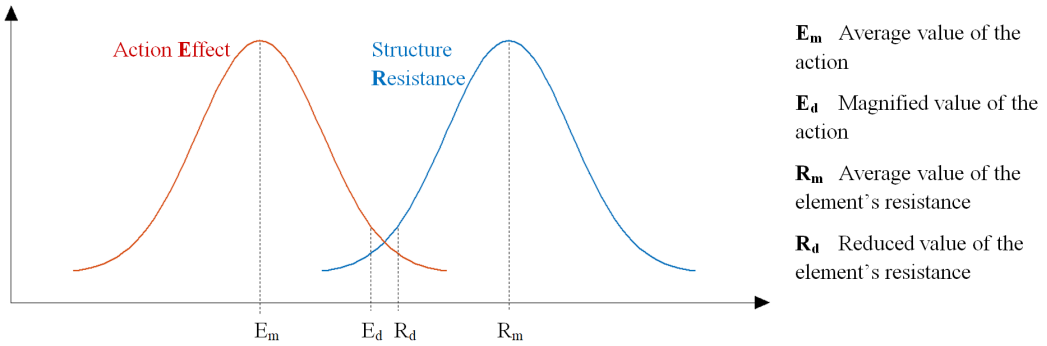

Figure 15: *Qualitative representation of the probabilities of obtaining certain values for the solicitations and resistance. It is assumed that the correct factoring of each parameter will always mean that $E_d \leqslant R_d$*

Ultimate limit state (ULS)
The definition of the conditions applied on the system is based on the ultimate limit state, the situation in which the structure loses its ability to carry load in the manner assumed in the structural design. Depending on the structure type, several organizations deliver guidelines about which recommended security coefficients and load factors should be applied during the design. According to ABS (2016), in its guide for design criteria in offshore steel structures, the total factored load, F_d, used to establish the design load effect, is determined as follows:

$$F_d = \gamma_{f,D} D + \gamma_{f,L} L + \gamma_{f,E} E + \gamma_{f,S} S \tag{16}$$

where

$\gamma_{f,*}$	load factor appropriate to the load categories, [*=D,L,E, or S]
D	value of permanent loads
L	value of variable loads
E	value of environmental loads
S	value of supplementary loads

The following table, extracted from ABS (2016), shows the load factors for both static (ULS-a) and combined loads (ULS-b). Static loads factors should be used when the structure considered is afloat or resting on the sea bed in calm water. Combined loading factors are used when D, L, and S factors are combined with relevant environmental loading.

Design Conditions	*Limit States*	*Load Combinations*					*Resistance Factors* γ_R
		Load Factors γ_{f^*} (* = D, L, E or S)				*Environmental Events*	
		D	*L*	*E*	*S*		
Static Loadings	ULS-a	1.50	1.50	--	1.00	No Environmental loads, calm water cases Variable loads to include those from maximum owner or manufacturer specified operational and functional loads including impact and dynamic response effects; see 2-1/3.5.3.	1.05
Combined Loadings	ULS-b	1.10	1.10	1.35	1.00	The design load cases are to consider: • Owner specified loads due to environmental events including inertial loads induced by the Unit's dynamic response • The loads resulting from transit	1.05

Figure 16: *Structure load combinations and corresponding load factors (γ_f) and Resistance Factors (γ_R) for Common Structures (ABS (2016))*

Serviceability limit state (SLS)
A Serviceability limit state (SLS) is a type of limit state that, if exceeded, produces a loss of functionality or deterioration of the structure, but not an imminent risk. It normaly deals with issues that could affect such things as:

- Deflections that may alter the effect of the acting forces.
- Excessive vibrations producing discomfort or affecting non-structural components
- Appearance issues
- etc.

This paper will focus its attention particularly in the deflection of the bars and columns. Another guideline about offshore standards with the title "Design of offshore steel structures, general - LRFD method" provides limiting values for deflection (δ_{max}) criteria (DNV-GL (2016)). For normal steel structures—without supporting or being made with other brittle materials—the recommendation is

$$\delta_{max} = \frac{L}{200}$$

where L is the span of the beam/column.

7.1.2 The Cross method

The moment distribution method or also known as Cross method (after Prof. Hardy Cross, who developed it in the 1930s) is an iterative structural analysis method intended for statically indeterminate (hyperstatic) beams and plane frames. The method includes procedures for cases when side sway occurs or not. In this thesis, the situation which is considered, with geometric and load symmetry, a no side-sway case applies.
The moment distribution procedure for a no side-sway frame case is summarized (Lindeburg (1999)):

- Step 1. Draw a line diagram representation of the structure to be analyzed.
- Step 2. Calculate the stiffness for each bar using the following expression:

$$K = \frac{4EI}{L} \tag{17}$$

  where E is the Young's modulus, I is the bar inertia and L is the bar length.

- Step 3. Calculate the distribution factor at each end of the bars, recording them on the drawing (step 1), by means of the following expression:

$$DF_i = \frac{K_i}{\sum_i K_i} \tag{18}$$

It is convenient to remember that DF=0 at fixed ends and DF=1 at simple supports. It will be considered that the portal frames are fixed at the end of the pillar, where they are penetrated into the seabed (DF=0 at that points).

- Step 4. Obtain the fixed-end moments (they are tabulated). Record the fixed-end moments on the drawing at the ends of each bar. In this report, only the situation of a uniform distributed load will be met, the fixed-end moments of which can be calculated as shown in figure 17.

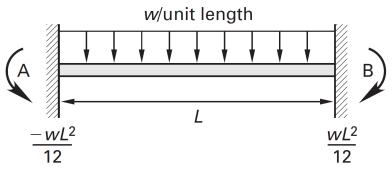

Figure 17: *Elastic fixed-end moment of a bar with a uniform distributed load (Lindeburg (1999))*

- Step 5. Go to any joint and calculate what is known as the "unbalanced moment", by adding all the moments at the ends of the bars that meet there. Afterwards, distribute the unbalanced moment to each bar; the distributed moments are equal to the product of the unbalanced moment times the distribution factor (computed in step 3) with the reversed sign.
- Step 6. Carry the distributed moment to the far end of the corresponding bar by multiplying the distributed moment by the carryover factor (β). A value of β =0.5 is normally used.
- Step 7. Repeat steps 5 and 6 until the unbalanced moment at the most unbalanced joint is insignificant (typically, less than 1% of the largest fixed-end moment, calculated in step 4).
- Step 8: Calculate the true moments at each bar end as the sum of moments that have been recorded at that end.

In order to easily calculate the moment, as well as the normal and shear force distributions, the software *Ftools* is used throughout this paper.

7.1.3 Determination of the states of stress at critical locations. Failure criterion

For reasons later explained, an I-beam, also known as H-shaped cross-section, will be used in the structure reinforcements. That is why the study of the stresses occurring in this kind of profiles is showed in this section, that is normal and tangential shear stresses (torsional shear stresses are not relevant in the locations where analytical calculations will be carried out). The horizontal elements of the **I** are flanges, and the vertical element is known as the web.

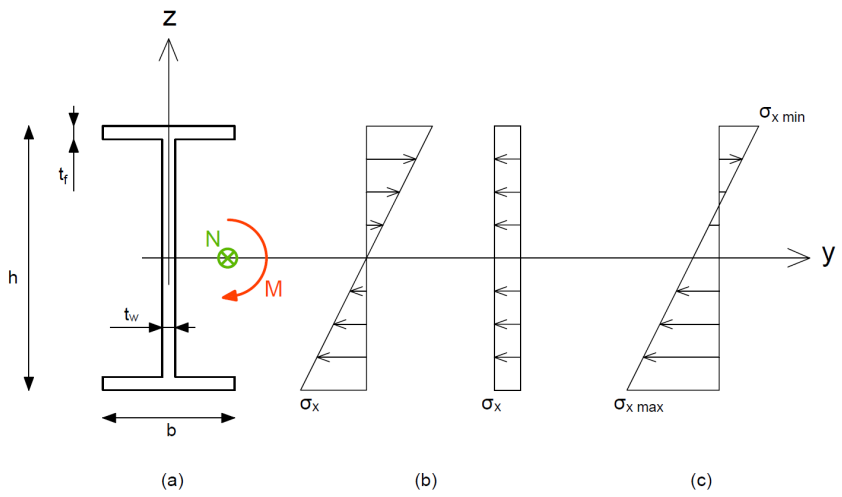

Figure 18: *(a)I-shape profile under bending and compression force. (b)Normal stress due to bending and compression σ_x. (c)Composition of both normal and bending stresses leading to a σ_{max} at the lower part in this particular case. A tensile normal force or a bending force with opposite direction would lead to different results. (Drawing done with Autocad 2018)*

Normal stress
Due to tensile/compressive (N) and bending forces (M), normal stress (σ) appear within a bars structure. The composition of both forces can lead to a asymmetric distribution of the normal stress, which has to be considered when analysing a section (see figure 18).

Tangential stress
Due to a tangential force, tangential stresses appear along the section (see figure 19).

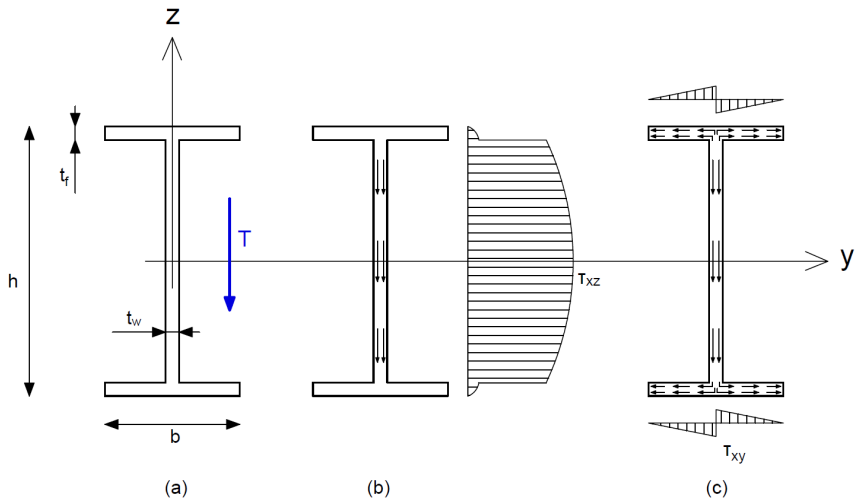

Figure 19: *(a)I-shape profile under tangential force. (b)Tangential stress τ_{xz} distribution. (c)Tangential stress τ_{xy} distribution. (Drawing done with Autocad 2018)*

The distribution of τ_{xz}, the vertical shear stress, has a great discontinuity in the transition from the flange to the web. As it can be seen in figure 19 (b), while in the flanges it is negligible, the web absorbs most of the T stress. Equation 19 is used to calculate these stresses at a certain point, where the first moment of area, m_y^A, is calculated as the area above that point, multiplied by its centroid.

$$\tau_{xz} = \frac{T_z m_y^A}{I_y t_w} \tag{19}$$

In addition to the tiny, and therefore negligible, vertical tensions that appear within the flanges, there are other horizontal ones that must be taken into consideration, τ_{xy} (see figure 19 (c)). Equation 20 is used to calculate these stresses at a certain point along the flanges, where the first moment of area, $m_y^{A'}$, is calculated as the area of flange from its edge to that point, multiplied by its centroid.

$$\tau_{xy} = \frac{T_z m_y^{A'}}{I_y t_f} \tag{20}$$

Failure criterion. Von Mises
This paper will analytically calculate those cases that can be assimilated as simple bending ($M_y + T_z$), plus any normal forces (compressive or tensile). In these cases, the stress tensor can be expressed as:

$$\sigma = \begin{bmatrix} \sigma_x & \tau_{xy} & \tau_{xz} \\ \tau_{xy} & 0 & 0 \\ \tau_{xz} & 0 & 0 \end{bmatrix}$$

Since steel will be the material used for the suction caisson, a failure criterion for ductile materials should be used.

$$\sigma_{eq.VonMises} = \sqrt{\sigma_x^2 + 3\tau_{xy}^2 + 3\tau_{xz}^2} \leqslant \sigma_{adm} \left(= \frac{\sigma_e}{\gamma_R} \right) \tag{21}$$

where γ_R is the reduction factor of the material resistance. As depicted in figure 16, $\gamma_R = 1.05$.

7.1.4 Optimum shape of a profile

When choosing a bar profile, the optimum situation is that in which the most amount of area is as separated from the bending axis as possible.
The geometric efficiency is defined as the profile inertia divided by the ideal profile inertia:

$$g.eff. = \frac{I_y}{I_{yi}}$$

where the ideal inertia is calculated as if the whole area was concentrated at the extremes. For instance, in a rectangular shape, applying the Steiner's theorem:

$$I_{yi} = 2\left(\frac{A}{2}\left(\frac{h}{2}\right)^2\right) = \frac{bh^3}{4}; \qquad I_y = \frac{1}{12}bh^3; \qquad g.eff. = \frac{1}{3}$$

where

A Rectangular section area
h Rectangular section height
b Rectangular section width

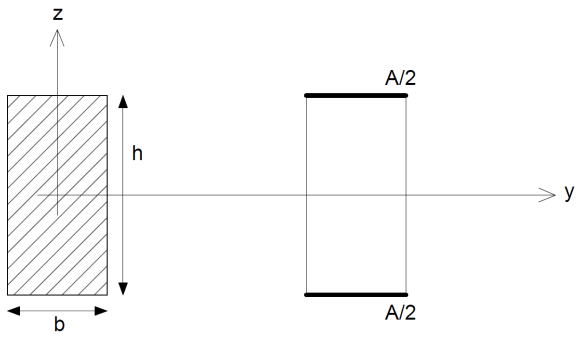

Figure 20: *Calculation of the geometric efficiency of a rectangular shape profile. (Drawing done with Autocad 2018)*

In table 5, a comparison between the geometric efficiencies of different profiles is depicted. Therefore, an I-shape profile is one of the most efficient profiles. That means that with a lower amount of material (smaller area), the same inertia can be obtained, thus the maximum stresses occurred within the section will be the same. That has the interest of this paper, since most of the time, optimizing the design will imply reducing the amount of material used for the structure.

Table 5: *Geometric efficiencies depending on profile shape. (Drawings done with Autocad 2018)*

Rectangular	IPN	Circular tub	Circular
1/3	2/3	1/2	1/4
	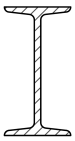	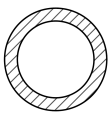	

7.1.5 Composite profiles

When a profile is made of diverse attached profiles, several parameters happen to be modified. This will be the case, since the external 3cm width steel sheet will have to be taken into account when carrying out the analytical calculations.

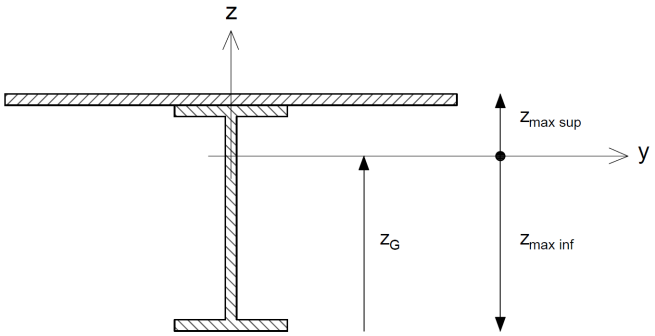

Figure 21: *Composite profile. (Drawing done with Autocad 2018)*

The neutral axis position varies and can be calculated as follows:

$$z_G = \frac{\sum_i (z_{Gi} A_i)}{\sum_i A_i} \tag{22}$$

The global inertia will also be affected (z_i being the inertia of each profile measured from the lowest surface of the composite profile):

$$I_G = \sum_i I_i + \sum_i A_i (z_G - z_i)^2 \tag{23}$$

7.2 Outline for the analysis

This section pretends to give a clear image of the path that will be followed within this section.
As mentioned in section 3, the suction caisson that the Ocean Grazer is developing should be able to work as an anchoring system not only for the energy storage structure and other harvesting platforms, but also as an independent suction caisson with multiple applications.
The design variations between both versions suggest that they should be divided in the following sections as different cases:

- Case I. Suction caisson conceived as an independent feature, able to provide anchoring to any application.
- Case II. Suction caisson particularly designed for the Ocean Grazer storage system.

7.3 Suction caisson Case I

Case I is the suction anchor though to be as an independent module, able to accommodate any sort of structure.

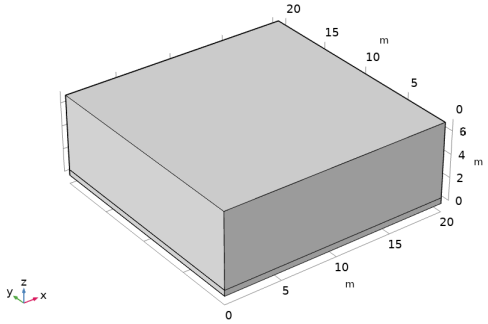

Figure 22: *Model used in simulation I.0 (drawing from Comsol Multiphysics v5.4)*

The initial model is a 20x20x7m caisson with a wall width of 3cm. The vertical effective force (i.e. the own weight minus any buoyancy effects) is estimated in 1923kN, which gives a self-weight penetration depth of 0,52m (equation and parameters used are detailed in sections 6.3.1 and 6.3.2).

7.3.1 Design I.0

This simulation intends to show that a reinforcement of some kind is needed, so that a structure with a span of 20 meters can resist. The simulation results at the middle of the span predict a Von Misses stress 10662 MPa and a displacement of 8m.

7.3.2 Design I.1

In order to get more stiffness, a model with transversal fins is analysed. A spacing of 50 cm between each fin is suggested.
The system will be assimilated as a rigid structural frame. Equally as a structural analysis, the load applied on each beam is assumed to be that applied on the surface defined by the beams spacing distance (see shaded area in figure 23); in this case, the surface considered will be determined by the fin spacing. Therefore, the simplification of considering a structure of T-shape beams, each one placed next to one another, is done. Assuming that the pressure on the walls will be 1,5 bars ($150kN/m^2$), a total 75kN/m will be applied ($150kN/m^2 \cdot 0.5$m).

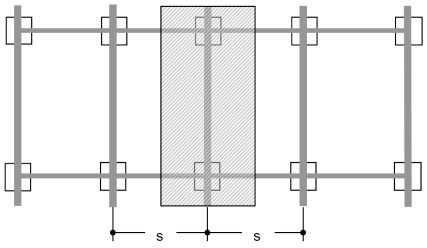

Figure 23: *Area accounting for each portal frame, defined by the separation s between frames (Lindeburg (1999))*

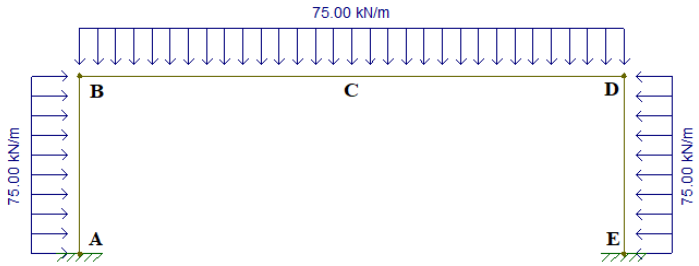

Figure 24: *Loads applied on the structure in design I.1*

An hyperstatic analysis will be implemented using the Hardy Cross method. Since we have a symmetrical loading, the analysis will only have what is known as a fundamental state. The penetrated part of the walls will be considered to be fixed.
Figure 25 shows the flector moment distribution obtained from *Ftools* software (based in the Cross method). In the middle point of the beam span (point C), there will be a moment of 1563 kNm, while it will have a maximum value of 2187 kNm at the extremes (points B and D).

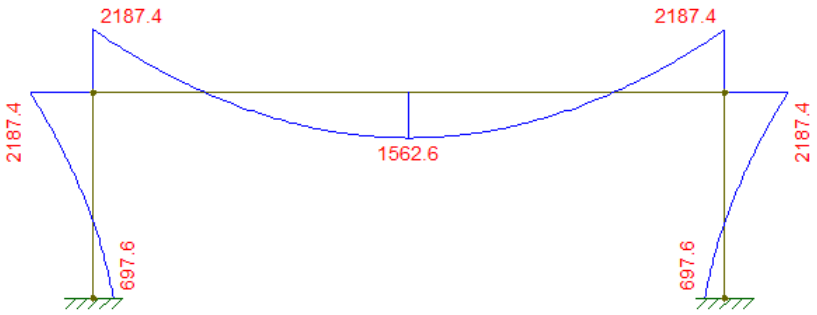

Figure 25: *Diagram of flector moments of design I.1 obtained from Ftools software*

A preliminary design of the fins is set to a 20 cm length and 2 cm width. ($A = 190cm^2; z_G = 19,08cm; I_y = 5622,15cm^4$)

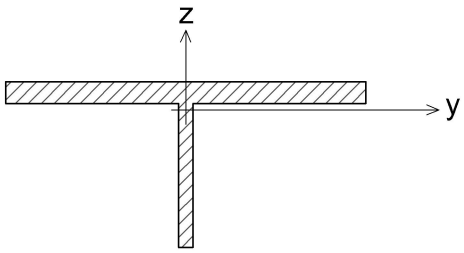

Figure 26: *Equivalent beam with T-shape profile (Drawing done with Autocad 2018)*

Assuming that simple flexion is applied on the beam, the Navier-Bernoulli law can be applied to obtain the normal stress distribution within the beam profile:

$$\sigma_{x,max} = \frac{-M_y}{I_y} z_{max} \tag{24}$$

The assumption of simple flexion will particularly not be true at the extreme of the beams, where a tangential stress will also apply. However, this is a simple calculation that aims to predict the results later obtained with Comsol.
Based on the profile parameters, equation 24 leads to a maximum normal stress of 5303 MPa (tension) at point C, while 7423 MPa (compression) at points B and D.
For further comparison and validation of the results found in the previous paragraph, a simulation using Comsol is carried out. A Von Mises stresses distribution is ploted, obtaining 5537 MPa at point C, and 6882 MPa at point C and D. Hence, the results are quite similar to those found analytically. The differences between each other are for various reasons. First of all, the equivalent Von Mises stress is calculated as the combination of the normal and tangential stresses in the principal directions, different in each point. Indeed, in point C, the tangential stress should be null, and the predominantly value is that of the 1st principal direction. However, values obtained with equation 24 did not take into account neither the contribution of normal component on the normal stress, nor the effect of the structure own weight, due to gravity. In points B and D, the differences are even greater for the fact that tangential stresses are substantial, and the point analysed not being exactly at the extreme, so that the results where not affected by the singularity at the corner. The concentration of tensions in this point will be discussed later on in this report. Additionally, and as an indication of improving with respect to design I.0, although insufficient, the maximum displacement is 431 cm (point C).
Therefore, we can conclude that the structural analysis is a correct first approach to predict the stresses that will occur, and hence, determine a design that would fit the requirements.
The results found in this design show that the reinforcement has to be improved substantially, which will be discussed in the following section.

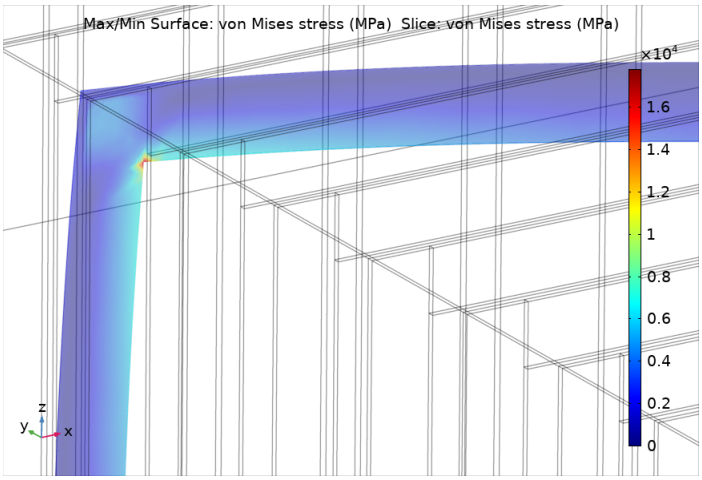

Figure 27: *Detail of the corner singularity. Von Mises stress diagram obtained with Comsol v5.4*

7.3.3 Design I.2

The results obtained in case I.1 are still far from the target. This means that a reinforcement profile with greater inertia should be considered.
Firstly, the necessary inertia of the reinforcements profiles should be determined. This has to be done in an analytical way. The results in the previous section show that indeed, the rigid frame analysis is a good approximation of the problem. In that case, part of the steel sheet of the caisson has been considered in each frame *beam*. However, literature show that this is actually a conflicting point to evaluate in this kind of problems: either consider the resistant sheet metal collaboration in the composite section or conservatively, limit its mission to distribute the loads and only tie the structural bar system. Henceforth the second modus operandi will be followed.
An I-shape beam is the most natural profile to consider, due to its geometric efficiency ratio. Specifically, an IPE profile will be taken into account. We suppose a class I profile, so that a platic criterion approach can be done. Therefore, $\frac{M_{y,Ed}^{max}}{M_{pl,Rdy}} \leqslant 1$ has to be met, where $M_{y,Ed}^{max}$ is the maximum moment occurring within the system, and $M_{pl,Rdy}$ the plastic moment of profile. Considering a maximum moment of 2187.4 kNm in points B and D, $M_{pl,Rdy} \geqslant 2187.4kNm$. The minimum section modulus ($W_{pl,y}$) can be obtained from the following expression:

$$M_{pl,Rdy} = W_{pl,y}\frac{f_y}{\gamma_{M0}} \tag{25}$$

Being $\gamma_{M0} = 1,05$ and $f_y = 355MPa$ for a S355 steel $\Longrightarrow W_{pl,y} \geqslant 6469 \times 10^3 mm^3$.
Checking a structural profiles catalogue, an IPE 750 x 196 would be necessary ($I_y = 240300 \times 10^4; W_{pl,y} = 7174 \times 10^3 mm^3; h = 770mm; b = 268mm; t_w = 15,6mm; t_f = 25,4mm; A = 251cm^2$).

A simulation is executed with this profile as reinforcements. A simulation of the overall structure accounts for an excessive amount of computational time. The fact that there is symmetry in terms of geometry and boundary conditions, a one plane symmetry is applied.

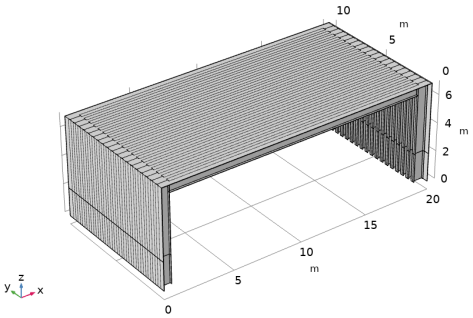

Figure 28: *Cut section of the design I.2*

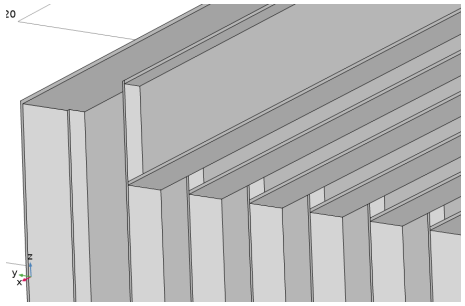

Figure 29: *Detail of the reinforcement in design I.2*

The results obtained are summarized in the following table, which shows that the structure will resist the solicitations (security coefficient around 1.4):

$\sigma_{eq,Mises}(C)$	211 MPa
$\sigma_{eq,Mises}(B,D)$	245 MPa
δ_C	6,7 cm

7.3.4 Design I.3

The previous design would mean an excessive reinforcement that would increase unnecessarily the weight and the cost of the system. That is why another solution is approached.
A division of the caisson in different compartments will lead to smaller spans, that consequently will inevitably decrease the moments that will be applied on the beams.
Likewise, the area of contact that will have to penetrate into the soil will also increase considerably. Besides, the movement of soil from the outside to the inside of the caisson will probably be affected as well. This will have consequences on the self-weight penetration depth and the underpressure needed during the suction-assisted penetration. The author of this thesis makes a series of assumptions, making some modifications to the equations used until now. It is important to make clear

that these changes are not neither experimentally nor analytically proved.
Both equations 9 and 11 have been used for the calculation. It is assumed that the calculation of the internal friction can be calculated equally for each compartment. Regarding the tip resistance, it is assumed that there can be movement of soil around the outer walls of the suction caisson, but not around the walls inside the caisson, this is the separator walls between compartments. Therefore, the vertical force will be calculated the same way in both equations, but adding the term referred to the tip resistance, used in conventional pile design practice (equation 31, appendix A). The equations will therefore become (changes are depicted in bold):

$$\begin{aligned} V' &= \gamma' Z_o^2 \left(exp\left(\frac{h}{Z_o}\right) - 1 - \left(\frac{h}{Z_o}\right)\right)(K\tan\delta)_o(P_o) \\ &+ \left(\gamma' \boldsymbol{Z_{i,c}^2}\left(exp\left(\frac{h}{\boldsymbol{Z_{i,c}}}\right) - 1 - \left(\frac{h}{\boldsymbol{Z_{i,c}}}\right)\right)(K\tan\delta)_i(\boldsymbol{P_{i,c}})\right)\boldsymbol{n_{w,c}} \\ &+ \sigma'_{end}(A_{end}) + \left(\boldsymbol{\gamma' h N_q} + \gamma' \frac{\boldsymbol{t}}{\boldsymbol{2}} \boldsymbol{N_\gamma}\right)\boldsymbol{A_{tip,c}} \end{aligned} \tag{26}$$

$$\begin{aligned} V' + s(\boldsymbol{A_{i,c}}\boldsymbol{n_{w,c}}) &= \left(\gamma' + \frac{as}{h}\right) Z_o^2 \left(exp\left(\frac{h}{Z_o}\right) - 1 - \left(\frac{h}{Z_o}\right)\right)(K\tan\delta)_o(P_o) \\ &+ \left(\left(\gamma' - \frac{(1-a)s}{h}\right)\boldsymbol{Z_{i,c}^2}\left(exp\left(\frac{h}{\boldsymbol{Z_{i,c}}}\right) - 1 - \left(\frac{h}{\boldsymbol{Z_{i,c}}}\right)\right)(K\tan\delta)_i(\boldsymbol{P_{i,c}})\right)\boldsymbol{n_{w,c}} \\ &+ \left(\left(\gamma' - \frac{(1-a)s}{h}\right) Z_i \left(exp\left(\frac{h}{Z_i}\right) - 1\right) N_q + \gamma' t N_\gamma\right)(A_{end}) \\ &+ \left(\boldsymbol{\gamma' h N_q} + \gamma' \frac{\boldsymbol{t}}{\boldsymbol{2}} \boldsymbol{N_\gamma}\right)\boldsymbol{A_{tip,c}}\boldsymbol{n_{w,c}} \end{aligned} \tag{27}$$

where

$Z_{i,c}$	The Z_i parameter calculated with the interior area and perimeter of a compartment
$P_{i,c}$	Internal perimeter of a compartment
$A_{i,c}$	Internal area of a compartment
$n_{w,c}$	Number of compartment walls
$A_{tip,c}$	Tip area of a compartment wall

Therefore, the same procedure followed in section 7.3.3 is carried out, using these equations.
As a first approach, the design consists of a total of 5 compartments, separated by 3 cm width walls equally spaced. In comparison to previous designs, in this case, the effective vertical force will vary, since the weight will be substantially increased. A similar approximation as the one at the beginning of section 7.3 is done, leading to a $V' = 3041kN$. That implies a self-weight penetration of 0,6 m and a subsequent suction needed of 1,18 bar. Although this initial penetration depth and underpressure are slightly greater, a value of 0,5m and 1 bar suction (1,5 bar for ULS) will be considered again.
Several combinations have been tried and a separation of 1 m between beams is decided in this case (150 kN/m applied on each frame). An initial separation of 0,5 m separation on the vertical reinforcements is maintained, to avoid high moments at the extremes of the structure. This leads to a moment distribution as depicted:

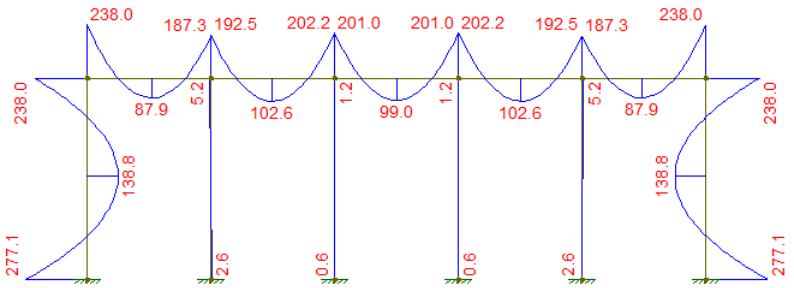

Figure 30: *Diagram of flector moments of design I.3 obtained from Ftools software*

Using equation 25, two different sections will be defined for the two outer frames (considering a maximum moment of 238 kNm) and another one for the three in the middle (maximum moment of 202.2 kNm):

- Two outer frames. IPE O 300. ($I_y = 9994 \times 10^4; W_{pl,y} = 743,8 \times 10^3 mm^3; h = 304mm; b = 152mm; t_w = 8mm; t_f = 12,7mm; A = 62,8cm^2$)
- Three inner frames. IPE 300. ($I_y = 8356 \times 10^4; W_{pl,y} = 628,4 \times 10^3 mm^3; h = 300mm; b = 150mm; t_w = 7,1mm; t_f = 10,7mm; A = 53,8cm^2$)

A Comsol simulation is carried out in order to prove that these profiles will resist the solitations.

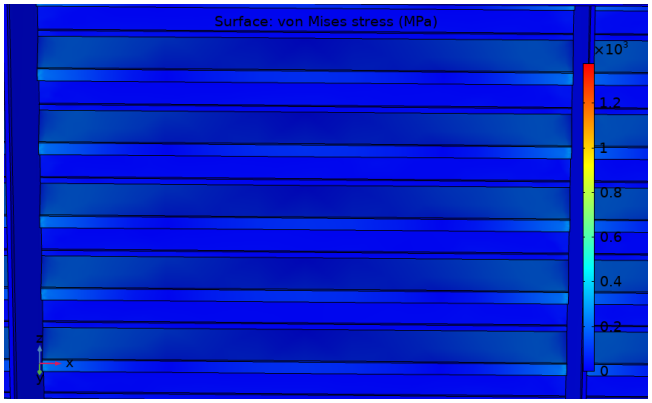

Figure 31: *Detail of the Von Mises stress distribution along a beam belonging to the central frame*

As it can be seen in figure 31, the maximum stress is found at the extremes of the beam, while this is not that relevant at the middle of the span. In the case of the central frame, the values found are 198 and 91 MPa, respectively, whereas at the outer frames, the values are 228 and 11 MPa. Therefore, taking into account a S355 steel the security coefficient in these reinforcements is about 1,7. Indeed, it is a relatively high value.

Vertical reinforcements

Until now, only the horizontal reinforcements have been checked. In that case, only the flexion due to the moments is considered, but the fact that all the walls are fixed makes that a normal force is also applied on the beams profiles that can induce a flexion, which has been neglected.
However, when designing the reinforcements, the possibility of buckling has to be considered. It will be done for the vertical reinforcements of this design, and for all reinforcements in the following sections.
Therefore, each column (as said before, a separation of 0,5 m is considered) of the outer walls, is affected by a composite flexion. Specifically, at its base, M=277 kNm and N=312.7 kN (compression). Hence, a formula of interaction between the two will be applied (see equation 28, the significance of each parameter is detailed in the next paragraphs), taking into account that this compression can lead to buckling. The possible lateral overturn phenomenon will not be taken into account.

$$\frac{N_{Ed}}{\chi_{min} A \frac{f_y}{\gamma_{M1}}} + \frac{M_{y,Ed}}{\frac{W_{pl,y} f_y}{\gamma_{M0}}} \leqslant 1; \quad where \ \chi_{min} = min\{\chi_y, \chi_z\} \tag{28}$$

In that case a HE profile is selected. Although their efficiency is inferior in comparison to IPE and IPN profiles, they have a remarkably higher critical load (N_{cr}) for the fact that both inertial moments are more balanced. That is why they are widely used in beams with certain flexion or pillars with moderate compression. Specifically the HEB 240 is used for the outer pillars ($I_y = 11260 \times 10^4; I_z = 3923 \times 10^4; W_{pl,y} = 1053 \times 10^3 mm^3; h = 240mm; b = 240mm; t_w = 10mm; t_f = 17mm; A = 106cm^2$).
For the buckling phenomena, a theoretical end restraint coefficent K=0.5 is considered as the bar is fixed at both extremes (see figure 32 (b)). Thus, the effective length $L_{cr} = KL = \frac{L}{2} = 6,5/2 = 3,25m$. The Euler's critical load (N_{cr}) can be calculated as follows (where E is the Young's

modulus, I is the pillar inertia):

$$N_{cr,y} = \left(\frac{\pi}{L_{cr}}\right)^2 EI_{pillar,y} = 22094 \times 10^3 N; \quad N_{cr,z} = \left(\frac{\pi}{L_{cr}}\right)^2 EI_{pillar,z} = 7697 \times 10^3 N$$

illus.	end conditions	ideal
(a)	both ends pinned	1
(b)	both ends built in	0.5
(c)	one end pinned, one end built in	0.707
(d)	one end built in, one end free	2
(e)	one end built in, one end fixed against rotation but free	1
(f)	one end pinned, one end fixed against rotation but free	2

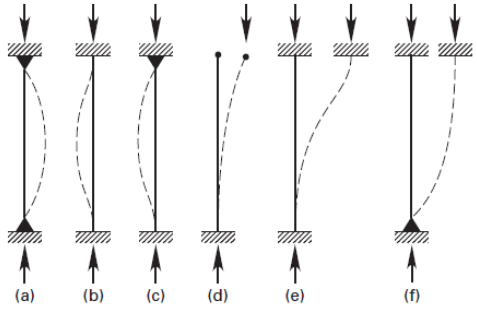

Figure 32: *Theoretical End Restraint Coefficients, K (Lindeburg (1999))*

What it is known as the reduced slenderness can be calculated as follows:

$$\overline{\lambda_y} = \sqrt{\frac{A_{pillar} f_y}{N_{cr,y}}} = 0,41 \tag{29}$$

$$\overline{\lambda_z} = \sqrt{\frac{A_{pillar} f_y}{N_{cr,z}}} = 0,70$$

where A_{pillar} is the section area of the pillar profile, f_y is the steel yield strength.

Using the calculated reduced slenderness ($\overline{\lambda}$) and the following graph, the buckling coefficient (χ) can be found. (The curves b and c should be used for the y and z axis respectively)

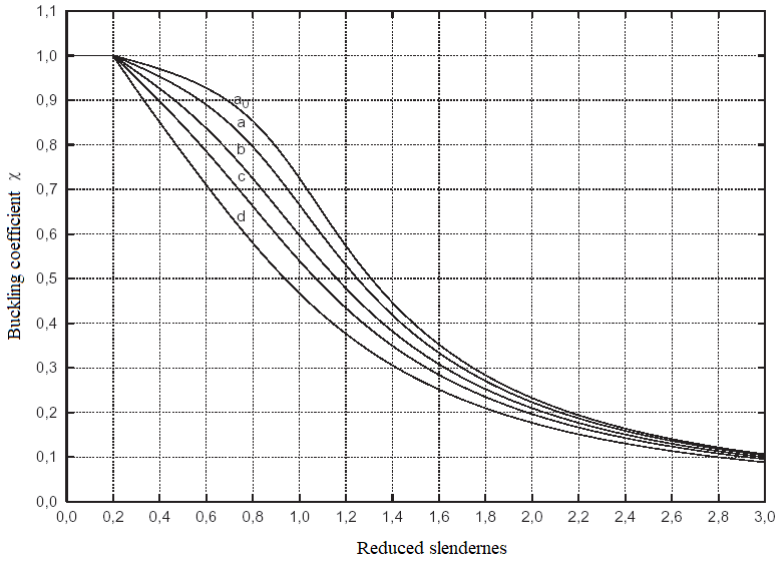

Figure 33: *Buckling curves (CEN (2005))*

Therefore:

$$\chi_{min} = min\{0,92; 0,73\} = 0,73$$

$$\frac{N_{Ed}}{\chi_{min} A \frac{f_y}{\gamma_{M1}}} + \frac{M_{y,Ed}}{\frac{W_{pl,y} f_y}{\gamma_{M0}}} = 0,12 + 0.78 = 89\%$$

which proves that the profile chosen (HE 240 B) is appropriate. As previously done, a simulation is carried out to prove that the stresses occurring along the structure will not lead to its failure.

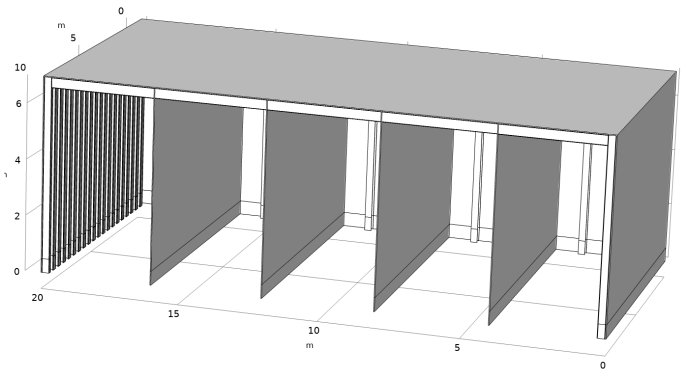

Figure 34: *Cut section of the design I.3 used in the simulation. Symmetry has been applied*

As expected, the highest stress will occur at the base of the pillars. A value at a height of 0,55m is taken, so that it is not affected by the singularity at exactly 0,5m, where a null prescribed displacement has been applied. For the beams used alongside the frames, the values obtained are around 245 MPa.

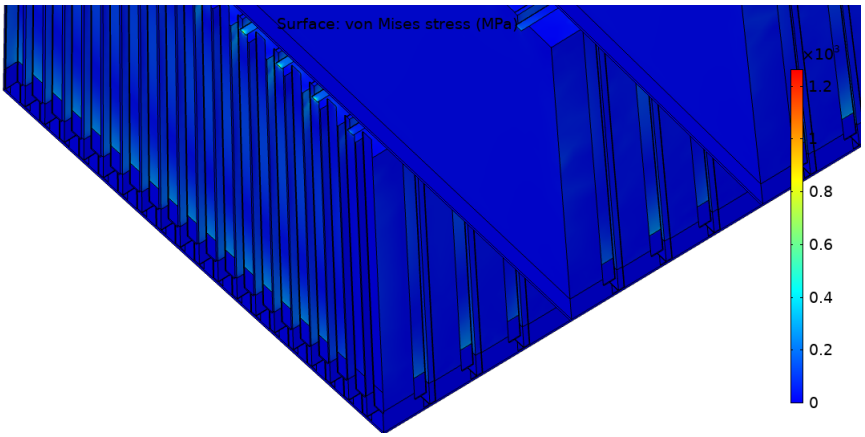

Figure 35: *Von Mises stress graph of design I.3*

7.4 Factorial design

The designs studied until the moment were carried out with boundary conditions and geometric parameters thought for very specific situations. For instance, on the one hand the soil properties where set to those that implied the most extreme solicitations. On the other hand, the separation between reinforcement frames was determined for different reasons. However, the variation of certain parameters like these would lead to different stresses and indeed, different designs.
A factorial design would allow to see which is the effect of each parameter of interest as well as the eventual interaction between each other.
A two level factorial design is implemented. Many variables will affect the outcome, but only those which are thought to be more relevant will be considered:

- Soil properties. They will affect the self-weight penetration depth as well as the suction required during the suction-assisted penetration. The following parameters will be taken into consideration as variable factors (the justification of each choice is backed by theory briefed in annex A.6):
  - Effective unit weight (γ'). Values between $8.19kN/m^3$ and $10.19kN/m^3$ account for very loose sand and very dense sand respectively.
  - $K \tan \delta$. K parameter and δ are always related to each other - considering them apart would not make sense. As it is depicted in annex A, there are different approaches to

calculate the lateral earth pressure coefficient. None of them, however, describes exactly the situation of a suction caisson installation.

- Angle of internal friction (Φ). Values between 30º and 45º account for very loose sand and very dense sand respectively.

One variable left in the formulation used is the permeability ratio k_f. It has been seen that its variation does not imply a major effect in the results. Furthermore, equally to the other parameters, its value should be determined by soil testing. A value of 3 is set for this case.

- Number of compartments in which the suction caisson is divided.
- Spacing of the reinforcements.

It is expected that there are no interactions between the soil parameters, so that they have an additive effect on the resistance against penetration. Therefore, the greater their values are, the greater the difficulty of the structure to be pushed into the soil. In order to prove such approach, a preliminary factorial study has been carried out with the variables previously depicted:

Factor	Name	Units	Low level (-)	High level (+)
A	Effective unit weight ($\gamma^{'}$)	kN/m^3	8,19	10,19
B	$K \tan \delta$	-	0.5	0.8
C	Angle of internal friction (ϕ)	[degrees]	30	45

Therefore, the two-levels factorial design will be implemented with the following factors:

Factor	Name	Units	Low level (-)	High level (+)
A	Sand properties	-	Loose sand	Dense sand
B	Number of compartments	-	1	5
C	Spacing of the beams	m	0.5	1

The total weight of the structure, depending on the design, has been considered as the main response for the analysis, for the fact that, as previously discussed, a lighter structure is desired for economical reasons. Depending on the factors that apply to every case, the best design is considered so that the strength and stability of the structure is sufficient to resist the expected solicitations. This designs, with their appropriate reinforcement, will have different total weights.

In order to carry out this study, the following steps and considerations will be followed:

1. Setting the relevant factors (A, B and C)

Preliminary stage

2. Assuming a certain preliminary effective vertical weight $V^{'}$
3. Calculating the initial self-weight penetration depth and suction needed in the suction-assisted penetration stage, by using equations 26 and 27.
4. Obtaining bending and normal forces diagrams, according to the Cross method. The section properties are set to be the same in all bars of the structure.
5. Setting a certain profile for all bars within the structure (i.e. beams and pillars)
6. Verification of the profiles by using equation 28, looking at the critical sections where the most severe stresses occur.

Iteration stages

7. Calculating the volume, and thereafter the new effective vertical weight $V^{'}$.
8. Idem step 3
9. Equally, the diagrams of bending and normal forces are obtained. However, in this case, each bar profile is specified, that is their dimensions and therefore, their inertia.

10. Checking if the profile still verifies equation 28, that is, its reinforcements are accurately defined. If not, a resizing should be done, and another iteration carried out.

Considerations and limitations

- When choosing the reinforcements, European standard profiles have been used. However, as previously explained in the theoretical section, each profile has its own geometric efficiency. The profiles used have different efficiencies, although they are certainly similar, for the fact that only section-type HEB has been considered. Therefore, it is assumed that the slight differences do not effect the result of the analysis.
- Equally, the security coefficient or utilization of the profile (calculated with equation 28 in step 6) also differ from one case to another. However, the differences effects are also neglected.
- The length of the skirt, as explained further up in the thesis, was set to 7m. According to calculations done in section 6, a minimum required length of 5.18m is necessary when installed in loose sand. Therefore, the structure is even more oversized for the case of dense sand, which could have an effect on the response which is being studied, the total weight of the structure.
- The considered suction to install the caisson is the maximum one. Therefore, improvements considered in design I.4 (see section 8.2) are not taken into account, but it is considered that the results could be extrapolated. Other minor design improvements and details are not accounted for either.

Results

Table 6 shows the response obtained in each "experiment", as well as the effects that each factor or combination of factors have in this response (see equation 30). Table 7 shows for each case the geometric efficiency and profile utilization. The purpose of displaying this data, as explained in previous paragraphs, is to state the fact that differences between each other will have an impact on the results, but they are neglected.

Table 6: *Test matrix with coded levels*

	A	**B**	**C**	**AB**	**BC**	**AC**	**ABC**	**Volume**
1	-1	-1	-1	1	1	1	-1	58,12
2	1	-1	-1	1	-1	-1	1	73,61
3	-1	1	-1	-1	-1	1	1	53,28
4	1	1	-1	-1	1	-1	-1	57,54
5	-1	-1	1	-1	1	-1	1	48,04
6	1	-1	1	-1	-1	1	-1	64,87
7	-1	1	1	1	-1	-1	-1	50,64
8	1	1	1	1	1	1	1	54,56
Effects	**10,13**	**-7,15**	**-6,11**	**3,30**	**-6,04**	**0,25**	**-0,42**	

Table 7: *Geometric efficiencies and bars utilization of profiles chosen in the factorial design*

	Central beam type	**Central beam g. eff.**	**Central beam utilization**	**Outer beam type**	**Outer beam g. eff**	**Outer beam utilization**	**Pillar type**	**Pillar g. eff.**	**Pillar utilization**
1	HE650B	69	99				HE550B	71	98
2	HE1000B	64	97				HE900B	65	82
3	HE160B	72	100	HE180B	73	86	HE220B	74	77
4	HE200B	73	84	HE220B	74	91	HE280B	75	91
5	HE1000B	64	98				HE800B	67	93
6	HL920x534	67	95				HL920x446	68	100
7	HE200B	73	100	HE220B	74	94	HE260B	75	91
8	HE260B	75	86	HE280B	75	100	HE400B	73	90

In order to investigate the main effects on the response, it helps to view the results in a cubical factor space. For instance, focusing on factor A (sand properties), the left side of the cube contains

the runs where A is at the minus level, while on the right side, the factor is at the plus level. Calculating the difference of averages of each level is known as the effect of factor A, which can be expressed as:

$$Effect = \frac{\sum Y_+}{n_+} - \frac{\sum Y_-}{n_-} \tag{30}$$

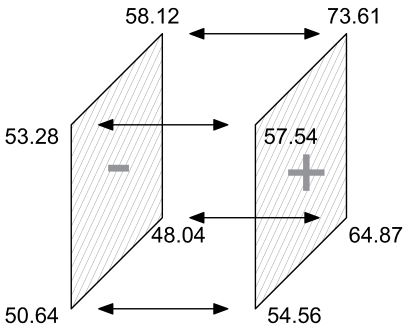

Figure 36: *Cube plot of total weights with focus on sand properties, factor A (Drawing done with Autocad 2018)*

Equally, this effect is calculated for all factors and combinations of them. The results are shown on the bottom line of table 6. If the effect is positive, it means that increasing that factor will makes the response (i.e. total weight) to increase, and the other way round when its value is negative. Notice that the most relevant effects are those of the factors, but also the interaction effect of BC, which is almost as high as its parents B and C. In other words, the combination of compartmentalization (B) and reinforcement spacing (C) produces a big (reducing) impact on total weight. The opposite effect (weight increase) happens, and to a lesser extent, with the interaction of dense sand (A) and high compartmentalization (B).
Interactions occur when the effect of a factor depends on the level of the other, and they cannot be detected by traditional one-factor-at-a-time (OFAT) experimentation.
In this case, tables 8 and 9 show the results for interactions BC and AB. These are actually averages of data from table 6, where for instance, the first two experiments have both factors B and C at their low level, with response values of 58.12 and 73.61, which produces an average of 61.81, as shown in table 8.

Table 8: *Data for interaction plot of nr. of compartments versus reinforcements spacing*

B	C	Volume (Avg)
-1	-1	61,81
1	-1	54,94
-1	1	53,57
1	1	52,6

Table 9: *Data for interaction plot of sand properties versus nr. of compartments*

A	B	Volume (Avg)
-1	-1	49,3175
1	-1	66,0605
-1	1	51,488
1	1	56,051

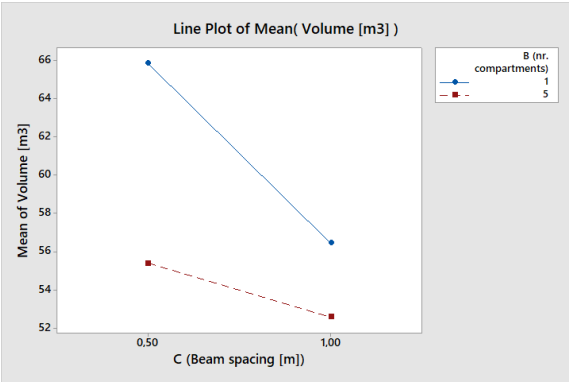

Figure 37: *Interaction of nr. of compartments (B) and spacing of the beams (C)*

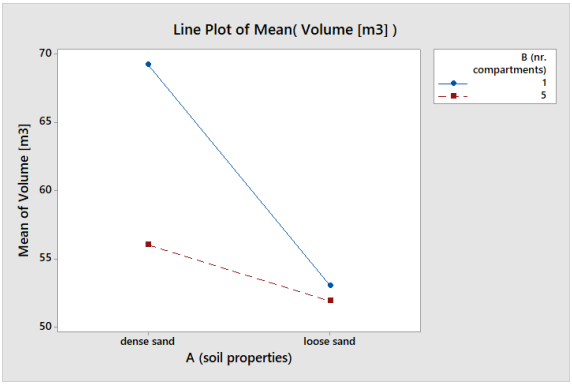

Figure 38: *Interaction of sand properties (A) and nr. of compartments (B)*

Notice that the effect of beam spacing (C), depends on the level of factor B (nr. of compartments). For example, when C is 1m (high level), the change in weight is small—from 53.57 to 52.6. However, when the beams are close to one another (C is at low level), the total weight is reduced considerably—from 61.81 to 54.94 (see figure 37, obtained with Minitab v18). Therefore, we can conclude that:

- If there is a high number of compartments in which the suction caisson shall be divided → changing the reinforcement spacing has little effect on the total weight of the structure.
- If the caisson is divided into a low number of compartments → increasing the spacing between reinforcements will dramatically reduce the total volume.

A similar situation is depicted for interaction of factors AB (see figure 38, obtained with Minitab v18). Equally:

- If the caisson is divided in a high number of compartments → the fact of being installed in dense or loose sand has little effect on the total weight of the structure.
- If the caisson is divided into a low number of compartments → installing the caisson in loose sand will considerably reduce the total volume, in comparison to a bucket placed in dense sand.

7.5 Unions

As previously discussed, the area concerning the union between the beams and the pillars demands special attention due to the concentration of stresses.
Connections are important parts of any metal structure. The mechanical properties of the unions greatly influence the strength, rigidity and stability of the structure as a whole.
In general, connections classification can be divided into flexible and rigid unions, depending on the ability of transmitting a significant moment or not. They could also be classified by the elements type that they unite—beams and columns mainly. In this case, a rigid union between beams and columns shall be designed.
In moment resisting connections like this, bolted end plate and welded beam-to-column connections are most commonly used. The welded connections can provide full moment continuity, but are certainly much more expensive to produce, specially on site. This report will not carry out research on the the convenience of using one or another in the Ocean Grazer suction caisson; therefore, design procedure of the connection members—let it be either bolts or welding—will not be implemented. A careful selection of this members can avoid the need for strengthening of the joint, which leads to a more cost-efficient structure. However, sometimes there is no alternative to strengthening the connection zones, which can be implemented with a range of stiffeners that will be detailed and studied in the following paragraphs.

Stiffeners
A usual simplification in rigid unions calculations consists in assuming that bending and normal forces are absorbed by the profile flanges, while the shear forces by the web.
In the connection of figure 39 (a), it can be seen that point D is under the effect of forces F_2 and F_4, which coming from the flanges of the profiles must be absorbed by a weaker section, such as the web. These traction or compression forces can induce web yielding or local buckling respectively. These failure modes can be decisive for a connection's capacity. Therefore, in order to avoid this concentration of stresses, the most generalized solution in frames without haunches consists in prolonging the frames of the beam and the column, as indicated in figure 39 (b).

If the ABCD web was not able to withstand the shear stress, the usual solution is to reinforce it with a diagonal stiffener (figure 39 (c)), instead of increasing its thickness.

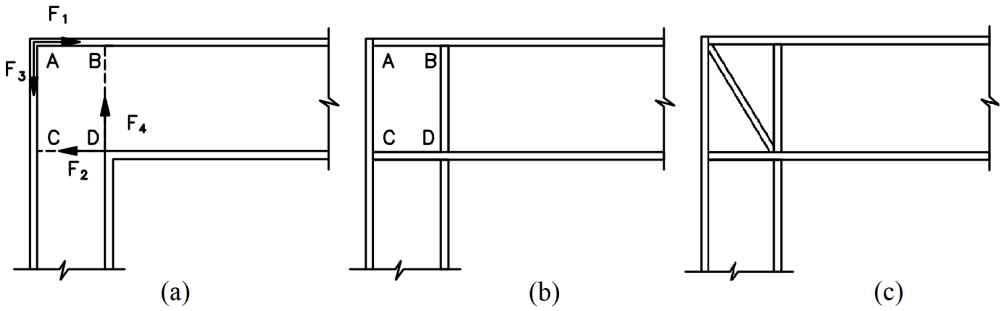

Figure 39: *(a)Forces transmitted from the flanges to the web (b)Stiffeners solution (c)'N' stiffener (UCLM (2005))*

Several simulations have been carried out in order to see the influence of introducing stiffeners in a beam-to-column connection as strengthening solutions.
Firstly, the 5-compartments suction caisson model is approached. Since in this case the span is 4 meters, a connection without haunches is firstly considered. Figures 40 and 41 show the comparison between a connection in which the beam is attached to the column's flange (as in the rest of simulations, a perfect union between solids is assumed), and the same connection reinforced with stiffeners. The higher stress, in both cases occurring at the lowest beam's flange in its very end, is dramatically reduced when stiffeners are present. For instance, in this case, their values are 1029 and 640 MPa respectively. The diagonal or 'N' stiffener, as previously explained, reduces the stresses occurring within the web, but it has a negligible effect on this maximum stress.

Table 10: *Higher equivalent Von Mises stresses comparison between FE simulations*

Without stiffeners	**With stiffeners**	**Haunch**		**Haunch + stiffener**	
		lower edge	upper edge	below edge	upper edge
1029.0 MPa	639.75 MPa	260.91 MPa	513.50 MPa	159.39 MPa	343.51 MPa

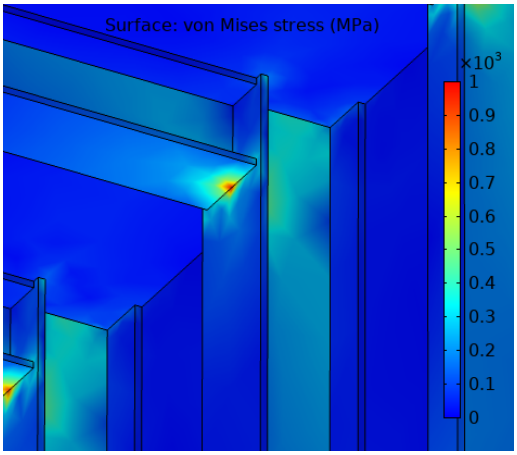

Figure 40: *FE simulation with Comsol of a connection without stiffeners*

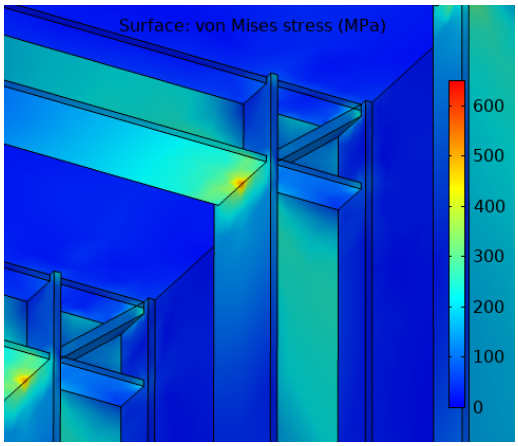

Figure 41: *FE simulation with Comsol of a connection with stiffeners*

Haunches

Although the usage of stiffeners reduces the concentration of stresses, the value encountered in this case with certain solicitations is still too high. That is why other solutions are investigated. In fact, in structures with long spans, the usage of other kind of reinforcements—mainly haunches—is recommended.
For portal frame structures, haunched connections at their eaves are widely used. In addition

to providing increased connection resistances, the haunch increases the moment resistance of the beam, which would obviously effect the optimization of the design and that will be discussed in later sections.
The haunch adds stiffness to the frame, reducing deflections, and facilitates an efficient moment connection. It is usually implemented as a triangular cutting placed below the beam at the connection to the pillar. Its length will generally be around 10-15% of the span, and is in most cases cut from the same section as the beam, or a deeper section.
As done with the stiffeners, some preliminary simulations have been carried out to see the impact that a haunch has on the stress distribution. The equivalent Von Mises stress distribution of the 5-compartments suction caisson with haunched connection without and with stiffeners is depicted in figures 42 and 43 respectively. As it should be expected, the maximum stresses are now concentrated around the haunch edges—values summarized in table 10. For instance, in this case, the haunch obviously reduces the stresses that occur within this region, with the stiffeners allowing to decrease this value to 343.51 MPa (close to the target for a S355 steel structure, where $\sigma_{VM,adm} = f_y/\gamma_R = 355/1.05 = 338MPa$).

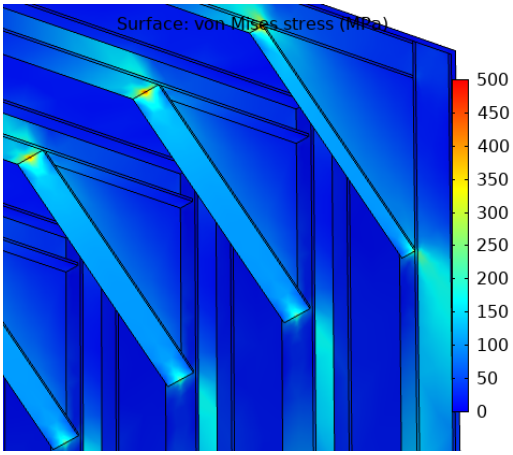

Figure 42: *FE simulation with Comsol of a connection with haunch*

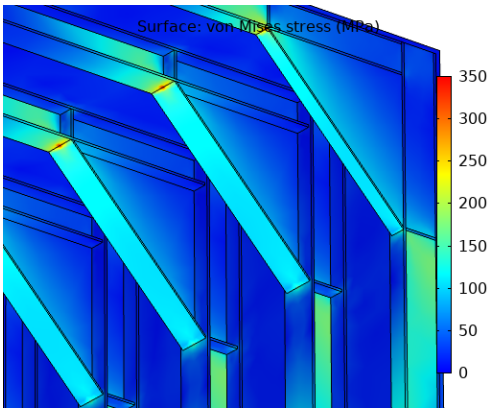

Figure 43: *FE simulation with Comsol of a connection with haunch and stiffeners*

Beam-to-column connections with haunch FE simulations
A series of simulations with a parametric sweep of a 1-compartment suction caisson with haunched beams has been done to see in which way haunches with different edge lengths effect the results.

Values between 1.5m and 2.5m (with a step increase of 0.2m) were given to both the vertical and horizontal haunch's edges, getting to 36 combinations in which the stress distribution around the beam-to-column connection was evaluated. Figure 44 shows the results, which have been rearranged in order to show those which would be acceptable (that is, with maximum equivalent Von Mises stress below the admissible stress $\sigma_{VM,adm}$)—the first 11 samples.

The results show that when increasing the vertical edge (y_h), while setting a fixed value of the horizontal edge (x_h), the haunch's upper edge will see stresses increasing, in opposition to the area around the lower edge, where the stresses will decrease.
Moreover, it can be concluded that similar values of (x_h) and (y_h) will give more stable and lower stresses. In contrast, highly different edge lengths will make the stresses to concentrate in one of the edges; if the reinforcement is vertically skinny, the upper region will have a high concentration of stresses, while they will appear around the lower area when the haunch has a considerably larger horizontal edge.

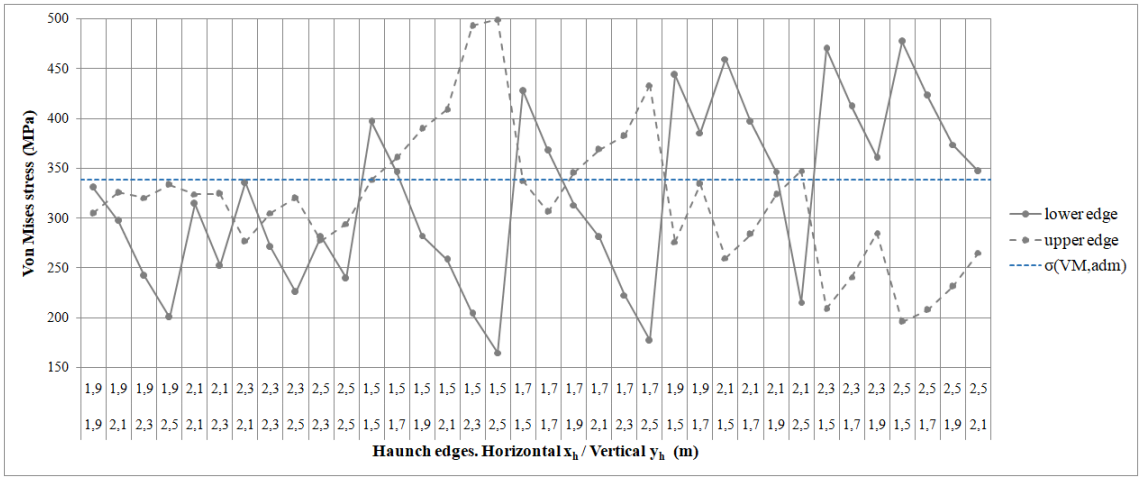

Figure 44: *Maximum equivalent Von Mises stresses in 1-compartment suction caisson with haunches*

The same approach has been followed for the case of a 5-compartments suction caissons. A parametric seep between 0.6m and 1.6m (with a step increase of 0.2m) was implemented for both vertical and horizontal haunch's edges. The results are similar, although, as it would be expected, the haunch dimensions can be reduced in comparison to the previous case (see figure 45).

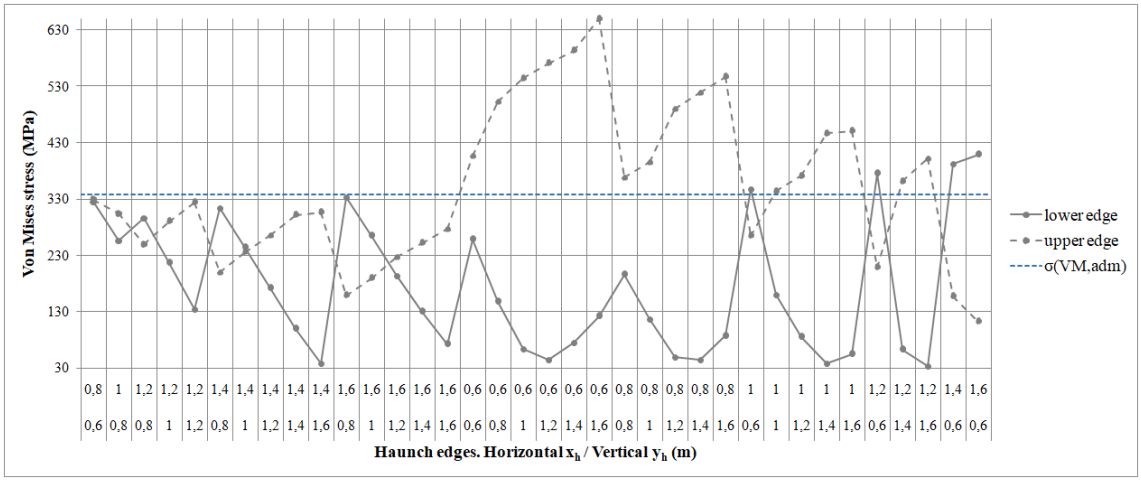

Figure 45: *Maximum equivalent Von Mises stresses in 5-compartment suction caisson with haunches*

7.6 Suction caisson Case II

The Case II is the suction caisson version that has been particularly studied and designed by the company so far, with the aim of providing an anchoring system for the Ocean Grazer storage system and other possible applications.

The design of each module is the same as Case I, but with a secondary upper portal frame attached to the main bucket. This secondary structure is 5 meters high and has a 10 meters span, surrounded by a rigid concrete tank at each side.

It is considered that on one hand, the suction pressure will be applied over all the inner surfaces of the caisson, including a quarter of surface of the concrete pipes. On the other hand, the ocean will make a pressure on the outside surfaces, which will vary with depth. As it has been proceeded in Case I, the simplification of considering the same external pressure will be done. Likewise, the maximum suction will always be taken into consideration.

Only the steel structure will be considered, and the effect of the concrete pipes will be applied

as external loads. This loads are simplified as a single vertical force, calculated as the weight of the structure and the water contained in it (assumed to be full in the installation process), minus any boundary effects (simplified as the volume of sea water removed). It is indeed an approximation, since a quarter of the pipe external surface will not be in contact with the ocean pressure, but will be under suction pressure. That will probably make this vertical force to increase, and a horizontal component will appear, which will be applied on the beams of the superior portal frame.

Table 11: *Values referred to concrete pipe*

$V_c[m^3]$	Concrete pipe volume	298
$V_w[m^3]$	Rigid tank volume	1272
$V_T[m^3]$	Total pipe volume	1571
$\rho_c[kg/m^3]$	Concrete density	2400
$\rho_w[kg/m^3]$	Working fluid density	997
$\rho_s w[kg/m^3]$	Sea water density	1020
$W_c[kg]$	Concrete pipe weight	716283
$W_w[kg]$	Working fluid weight	1268528
$W_T[kg]$	Total weight	1984811
$F_W[kN]$	Force due to weight	19471
$F_B[kN]$	Buoyancy force	15718
$F_T[kN]$	Effective vertical force due to concrete pipes	3753

The same procedure of the factorial design is followed but only for the case of loose sand, 1 m spacing between reinforcements and 1 compartment (which would equal to run 5 of the factorial design, where profiles of HE1000B and HE800B have been found necessary for the beams and pillars respectively).

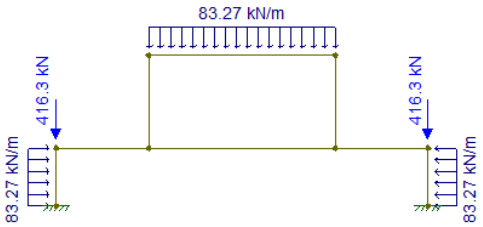

Figure 46: *Case II boundary conditions. 1st iteration*

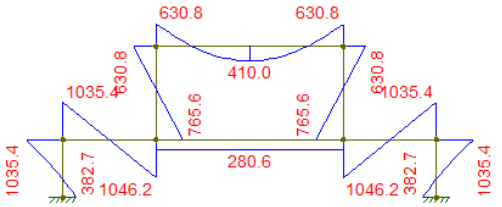

Figure 47: *Case II bending moments diagram. 1st iteration*

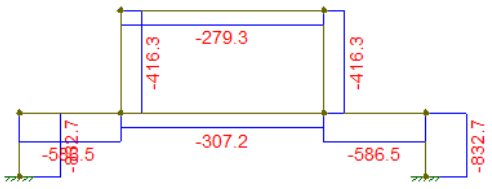

Figure 48: *Case II normal forces diagram. 1st iteration*

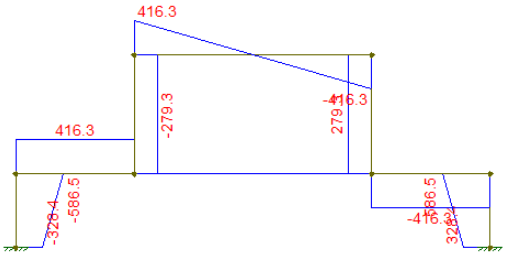

Figure 49: *Case II shear forces. 1st diagram*

The profiles that have been determined according to the Cross method are:

- Pillar main portal frame: HE450B with a 88,74% utilization.
- Beam main portal frame: HE500B with a 93.25% utilization. As it can be seen in the force distribution diagrams showed above, the central part of this beam experience lower solicitations. However, it has been considered the maximum values found at the extremes to decide the profile.

- Pillar secondary portal frame: HE360B with a 91.66% utilization.
- Beam secondary portal frame: HE340B with a 96.65% utilization.

Therefore, the profiles found are considerably smaller compared to those found in Case I. That is mainly because the effective vertical stress is higher due to the increased weight of the structure, due to the concrete pipes and the steel buckets. That has an impact in the self-weight penetration which is increased to 3.9m and the suction required in the suction-assisted penetration stage, which is reduced to 0.83 bar.

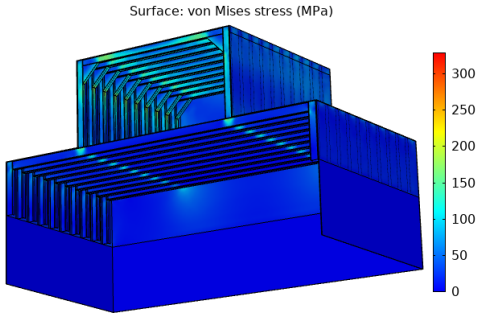

Figure 50: *Case II FE model. Equivalent VM stresses distribution*

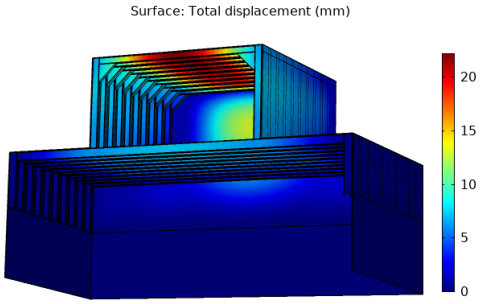

Figure 51: *Case II FE model. Displacements distribution*

On the one hand, as it can be seen in figure 50, the stresses along the superior caisson are more important than those occurring within the inferior one. That is probably due to the fact that a larger part of the inferior portal frame has been oversized, as it has been commented before and as it is depicted in the diagrams above. Its highest stresses are around the area of the beam where the upper pillars rest, where the highest bending moment occurs.
On the other hand, and in accordance with previous designs, haunches have been included in the upper portal frame of the model. The fact that this is a short span case, it could be possible that some stiffeners were enough.
The deflection diagram has also been included in order to prove that SLS is also met. The superior beam, with a maximum deflection of a bit more than 20 mm is far below the admissible value ($\delta_{max} = 50mm$).

7.7 Analytical validation of the models

Throughout the previous sections, various models have been developed in order to study and design different configurations of the suction caisson of the Ocean Grazer.
In this section, a validation of these models will be carried out by means of analytical methods and calculations, which have been summarized previously in the theoretical background section.
Particular cases of the 1-compartment and 5-compartments are looked carefully (run 5 and 7 of the factorial design, look appendix B for details), in which different points are analysed and compared to those results obtained with FEA.
As it has been previously discussed, the connection between the beam and the pillar has to be stiffened by means of different possible solutions, so that the admissible stress is not surpassed in the surroundings of this area. However, when introducing this elements, the analysis of the structure is modified. If the distribution of forces (that is axial, shear forces and bending moment) used in the factorial design for these particular cases are to be used, no haunches or stiffeners can be included in the model. The reason for this is that in order to obtain these forces, calculated with the Cross method, it has been assumed a uniform profile for each bar (i.e. beams and columns). When haunches are present, the composite profile is modified, and therefore the values of these forces change. Figures 52 and 53 clearly show that the section at the middle of the beam span sees lower stresses when haunches are included in the design.

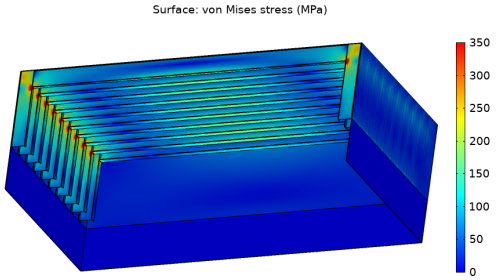

Figure 52: *FE simulation with Comsol of run 5. Von Misses equivalent stress distribution*

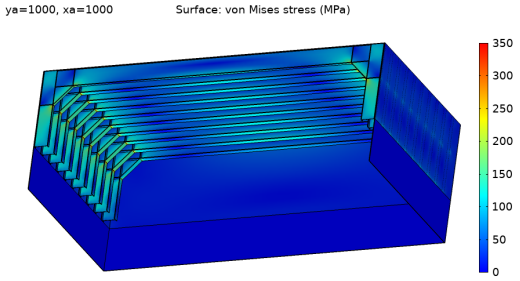

Figure 53: *FE simulation with Comsol of run 5 with haunch reinforcements. Von Misses equivalent stress distribution*

7.7.1 1-compartment case

Central section of the beam (Beam - Centre)
On the central section of the beam (which has a HE1000B profile), an axial (compression) force (-1102.4 kN) and a bending moment (2346.2 kNm) are applied (see figures 86 and 85, appendix B), while no shear forces are present (see figure 54).

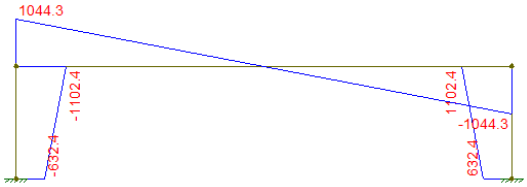

Figure 54: *Shear force diagram run 5, 1st iteration*

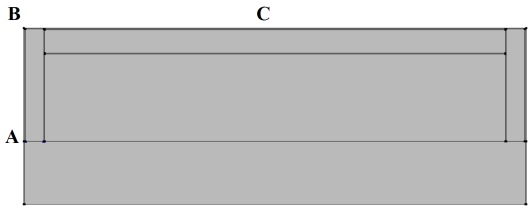

Figure 55: *Nodes assignation of end bars studied sections*

The results obtained in the FE simulation when no haunches are present in the design, and those obtained by analytical calculations are compared. As explained in section 7.1.3, in a composite profile like this, where not only the beam but also the 3cm metal sheet is accounted for, the neutral axis changes its position, resulting in the higher stresses occurring at the lower part of the profile. Thus, that is the point which will always be evaluated.

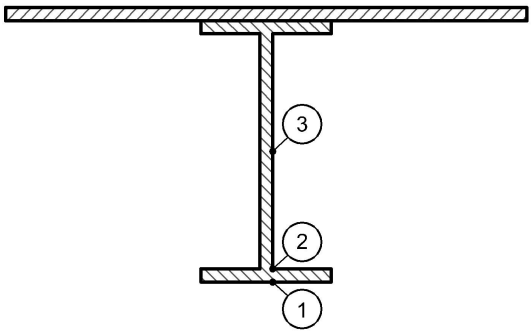

Figure 56: *Analysed points of the profile when a shear force is present (drawing done with Autocad 2018)*

Central section of the pillar (Pillar - Centre)
Unlike the beam, in that case, a part from a bending moment and normal force, on the central section of the pillar (which has a HE800B profile) a shear force is also present. Therefore, 3 points will be analysed: point 1 (outer surface of the flange which is situated the furthest from the neutral axis), point 2 (inner surface of that same flange) and point 3 (central point of the I-shape profile web). The reason for looking at these points and not others is due to the shear stress distribution, depicted in figure 19. Depending on the magnitude of the shear force and bending moments, the point where the maximum stress is occurring will vary.

End section of the beam (Beam - Node B)
This is the section which is affected by the highest bending moment, so probably, the section with the most severe solicitations.
It is clear that the connection of the model without haunches is not resistant enough, so there is no interest in any validation of the stresses at that area. Regardless of this, it is still interesting to look at a section close to this region, but far enough so that the results are not influenced by this concentration of stresses.

End sections of the pillar (Pillar - Nodes A and B)
The same approach is followed to find the stresses around the extremes of the pillar.

Table 12: *Comparison between FE simulation and theoretical stresses and displacement values across the run 5 model (1 compartment)*

Bar	Section	Avg FE stress (MPa)	Avg FE disp. (mm)	Theoretical stress (MPa)	Theoretical disp. (mm)	Rel. error stress (%)	Rel. error disp. (%)
Pillar	Centre p1	73.3	1.5	83.6	1.8	12	18
	Centre p2	106.4	1.5	91.4		-16	18
	Centre p3	118.7	1.5	87.1		-36	16
Beam	Centre	164.8	40.7	141.2	56.6	-17	28
Pillar	Node A p1	29.4	0.8	25.9	0.6	-14	-39
	Node A p2	73.8	0.8	44.6		-65	-39
	Node A p3	100.8	0.8	66.9		-51	-40
	Node B p1	137.5	2.0	148.4	2.0	7	0
	Node B p2	153.8	2.0	149.1		-3	-1
	Node B p3	135.4	2.0	104.3		-30	-2
Beam	Node B p1	87.3	8.8	84.1	13.2	-4	34
	Node B p2	102.2	8.7	86.0		-19	34
	Node B p3	101.4	8.1	68.6		-48	39

7.7.2 5-compartments case

Equally to the 1-compartment case, central sections of beams and pillar as well as their extremes are analysed, with values depicted in table 13.

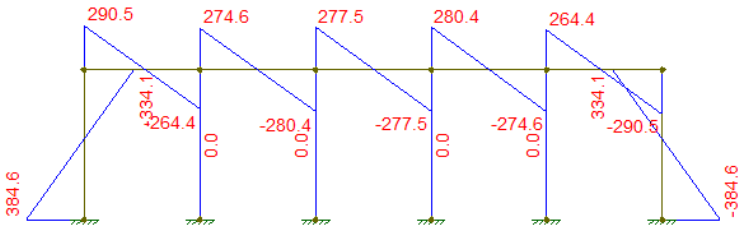

Figure 57: *Shear force diagram run 7, 1st iteration*

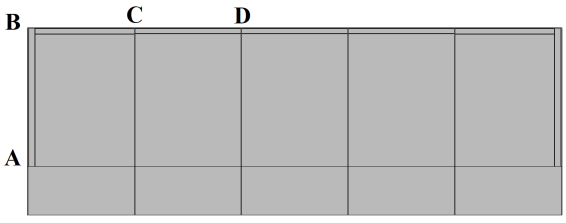

Figure 58: *Nodes assignation of end bars studied sections*

Table 13: *Comparison between FE simulation and theoretical stresses and displacement values across the run 7 model (5 compartments)*

Bar	Section	Avg FE stress (MPa)	Avg FE disp. (mm)	Theoretical stress (MPa)	Theoretical disp. (mm)	Rel. error stress (%)	Rel. error disp. (%)
Pillar	Centre	121.3	7.1	121.8	11.7	0	39
Outer beam	Centre	78.7	3.1	75.9	4.7	-4	34
Inner beam	Centre	132.3	5.9	126.0	9.6	-5	38
Central beam	Centre	119.5	5.3	118.0	8.6	-1	38
Pillar	Node A p1	75.8	2.3	101.7		25	8
	Node A p2	176.7	2.3	134.6	2.5	-31	9
	Node A p3	194.0	2.2	135.4		-43	11
	Node B p1	28.9	2.8	61.2		53	43
	Node B p2	134.8	2.8	101.8	4.9	-32	44
	Node B p3	159.0	2.7	115.3		-38	45
Outer beam	Node B p1	56.3	0.7	68.9		18	63
	Node B p2	149.3	0.7	102.7	2.0	-45	63
	Node B p3	158.8	0.7	111.1		-43	62
	Node C p1	68.7	1.4	86.7		21	31
	Node C p2	159.6	1.3	117.9	2.0	-35	32
	Node C p3	168.0	1.3	121.2		-39	34
Inner beam	Node C p1	76.5	2.1	98.4		22	33
	Node C p2	193.3	2.1	139.6	3.2	-38	33
	Node C p3	204.6	2.1	147.1		-39	34
	Node D p1	101.1	2.1	111.3		9	25
	Node D p2	206.8	2.0	150.2	2.7	-38	25
	Node D p3	213.5	2.0	153.7		-39	27
Central beam	Node D p1	97.1	1.8	109.8		12	26
	Node D p2	203.6	1.8	147.7	2.4	-38	26
	Node D p3	208.8	1.8	150.7		-39	28

7.7.3 Results

Tables 12 and 13 show the comparison between theoretical and FEA stresses and deflection values. The values of the FE simulations are an average of all the portal frames within the suction caisson. First of all, as explained before, these are not the maximum stresses that occur within the models, since these would be at the connection between beams and columns, which have not been included in the comparison. Therefore, the stresses showed should easily meet the condition in equation 21; thus the stresses should be no higher than $\sigma_{VM,adm} = f_y/\gamma_R = 355/1.05 = 338MPa$.
Also, taking into account the SLS limit of $\delta_{max} = \frac{L}{200}$:

- 1-compartment. The beam, being 20 meters long, should have a deflection no greater than 100 mm. The pillar, being 4.5 meters when starting penetrating, a $\delta_{max} = 22.5mm$ applies.
- 5-compartment. Every beam, being 4 meters long, should have a deflection no greater than 20 mm. The pillar, being 5.2 meters when starting penetrating, a $\delta_{max} = 25.9mm$ applies.

As it can be seen, these conditions are met, which also proves the usage of the Cross method and the whole procedure used throughout this paper to define the different designs is appropriate.

When analyzing the results, it has been seen that while in some sections of the structure (such as the center of the span), there is a smooth distribution of the stresses in the intersection between the flanges and the web of the I-profile, in other sections, the equivalent V.M stress changes abruptly, with the flanges merely supporting any stresses (such as the section where the bending moment is nul, see figures 59, 60 and 61).
This is, in fact, backed by the theoretical analysis. On one hand, when there is a bending moment and normal force applied on the section but no shear force—such as the centre of the span—, there is a progressive normal stress distribution from the neutral axis to the furthest point of the section (see figure 18); on the other hand, when the tangential force is the dominant—such as the section of the beam where there is no bending moment—, the web will see a mostly homogeneous shear

stress τ_{xz}, while the flanges will mainly absorb a neglectable portion of τ_{xz}, and τ_{xy}, always much smaller than the first one.

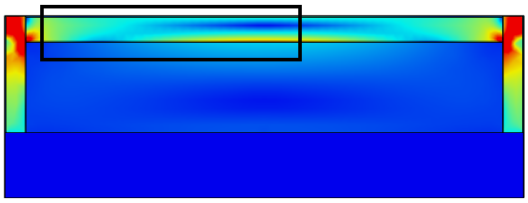

Figure 59: *Equivalent Von Mises stress distribution of run 5 model*

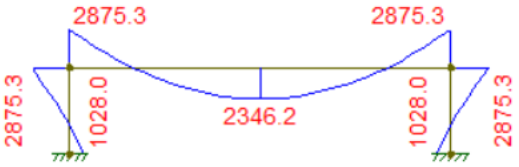

Figure 60: *Bending moment diagram run 5, 1st iteration*

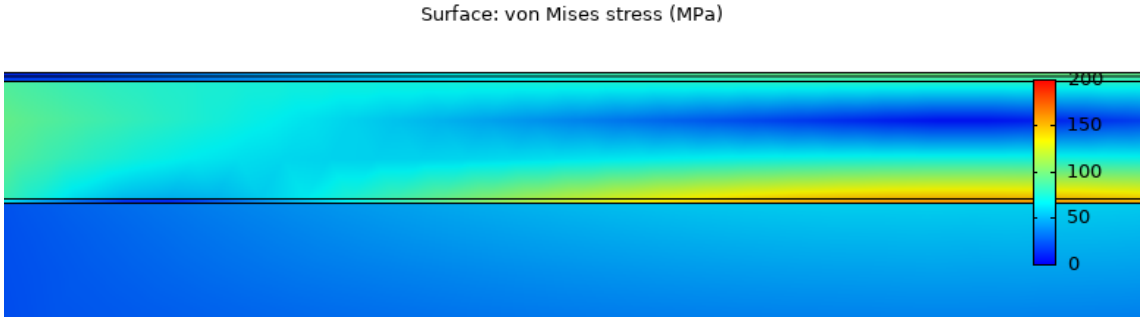

Figure 61: *Detail of the equivalent Von Mises stress distribution of run 5 model, see figure 59*

In order to show more clearly the comparison between theoretical and FE values, the relative errors have been calculated, taking the FE values as reference.
First of all, if we focus on the stress values, it is clear that when analysing different points of the same section, point 1 is generally much better predicted than points 2 and 3. That could be due to the fact that it is a not a symmetrical section, which it makes it harder to foresee. Likewise, it can be seen that point 1 always has a greater value when analytically calculated, and vice-versa for points 2 and 3.
Another conclusion that can be reached is that values in the centre of a bar are anticipated in a better way (especially in the 5-compartments case where absolute errors are no greater than 5%, but also in the 1-compartment case, where the relative error of the analysed sections (point 1) are as great as 17%). On the contrary, values at the extremes of the beams and columns are worse predicted, which can be explained by various reasons. First of all, it is possible that the studied section is too close to the connection and therefore, still affected by the concentrations of stresses. Another reason for this is that when carrying out the theoretical calculations, it has been assumed a frame of 20 meters length and the corresponding height, while it would have been more appropriate to take into account the neutral axis. It is possible that the normal and shear forces and bending moments used for the calculations and extracted from the diagrams are not accurately retrieved.
In terms of the deflections, with some exceptions most of the values are certainly badly predicted. When analytically calculated, it is assumed that the structure connections are completely rigid. However, this is not the case when haunches are included, not to mention when no haunches or other types of stiffeners are present, which is the case. That could be an explanation for these differences.

8 Discussion and conclusions

8.1 Discussion

This report deals with the search for design solutions for the suction caisson of the Ocean Grazer's storage system. First of all, research about this technology has been carried out, confirming that most of the cases consider cylindrical suction buckets. Methods found in literature to calculate holding capacity and installation procedures have been studied and adapted to the rectangular shape, taking into account size requirements specified by the company. Obtaining the self-weight penetration and the suction for the suction-assisted penetration stages will provide the main information for the boundary conditions that will be later used in the design procedure.

Different designs have been developed, dealing with the need for certain types of reinforcements in the structure, the main core of the thesis. Theoretical methodology of structural mechanics and design is depicted and used in order to calculate these reinforcements, assimilated as portal frames. Once the design is decided, FE simulations have been carried out with the aim of validating its resistance.
The first approaches provided information of the amount of stiffness that was needed and proved that simple plates or T-shape profiles lacked the required inertia and therefore were not a viable solution. For that reason, it was considered that an I-shape profile was the best approach for this case. At the same time, the methods for the suction caisson installation procedure were adapted again, to take into account the presence of this reinforcements and their effect on the resistance against penetration into the seabed.
While proving that the layout defined until the moment would be appropriate in terms of resistance (missing some details developed later in the report), it was also clear that the amount of required reinforcements was certainly high. For that reason a compartmentalization could be a solution to reduce the size of the profiles. By means of a third modification of the installation procedure methods, it was proved that indeed, the division of the suction caisson allowed the reinforcements to be reduced in size. However, it was not clear if these changes had an impact in the amount of material of the whole structure.
The designs done until the moment were based in certain conditions and parameters arbitrarily chosen. A two level factorial design was implemented with soil properties, the number of compartments and the spacing of the reinforcements as factors. It was concluded that all of them had a remarkable effect on the volume of the structure. It was trivial to see that looser sand would decrease the reinforcement, while it was not that straight forward that increasing the number of compartments or the distance between reinforcements would also reduce it. However, the factorial design allowed to see that some interactions between these factors existed. Beam spacing and loose sand had a remarkable impact on the decrease of volume only when the number of compartments was small (i.e. a single caisson).

In the previous designs and procedures, the concentration of stress occurring within the connection between bars was neglected. Stiffeners and haunches are presented as possible solutions. Although the cases analysed implied the need of haunches, stiffeners proved to be good and simpler solutions when the solicitations are not that extreme. As said in literature, FE simulations show that haunches length and height a 10-15% of the span is necessary, with no much differences between the two dimensional parameters.

Without going in depth in it, the analysis of another case has been carried out, where a secondary portal frame was included and the presence of the rigid concrete reservoirs was taken into account. The fact that the effective vertical force was more than doubled, mainly because of the concrete weight, the suction was easier to perform, and therefore, less stiffening was required.

Finally, a validation of the results obtained with FEA have been compared to those calculated by theoretical methods and calculations.

8.2 Further work

This thesis is a first glimpse of which are the possibilities for the design of the Ocean Grazer suction caisson. Further research that it is considered important in next steps is depicted in the following sections.

8.2.1 Cylindrical suction caisson

This thesis assumed since its beginning the design that was being developed by Ocean Grazer at that moment, which is essentially different to the cases found in literature for its rectangular shape. A comparison between a cylindrical and an equivalent rectangular shape could be of the interest of the company in order to make a decision on the convenience of using one or the other.

8.2.2 Design I.4

In this report, the boundary conditions applied on the model have been simplified. As previously explained, in an attempt to make the model more simple and at the same time get conservative results, the maximum suction needed is applied at all times. However, this is not what actually happens, making the design oversized. As it can be seen in figure 12, the suction needed at the first stages of penetration is much lower, increasing with penetration depth.
With the intention of improving the solution, thus using the least amount of material that makes the structure resistant enough, another approach could be followed.
If the loading effects that will occur on the structure along the whole process of penetration are plotted, it can be seen that at the very fist stages, the reinforcement required is much lesser than that needed once the caisson is almost anchored. In the latter, however, the skirt will be mainly buried into the soil.
If the load effects on the structure are considered at all times to decide on the reinforcement profile dimensions along the skirt height, this will inevitably lead to an increasing area of the pillars from the skirt tip to the top (see figure 62).

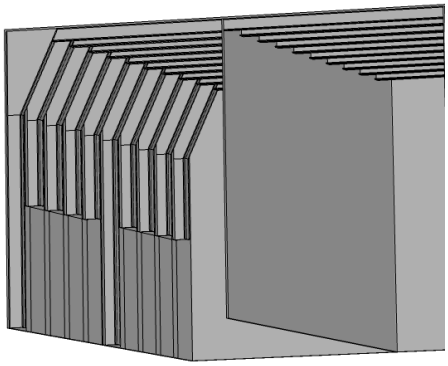

Figure 62: *Detail of a possible implementation of a non-uniform reinforcement layout*

8.2.3 Suction caisson life stages other than installation

As depicted at the beginning of the report, the suction caisson will go through different stages before and after its installation. In this report it has been considered that the most severe conditions which the structure will suffer will be during the installation procedure. However, the complete design should include the rest. The operational stage is particularly interesting, probably more in the light of the holding capacity of the caisson than the resistance of the structure. This thesis has performed stationary simulations with perfect anchoring of the suction caisson into the sand, and no relative movement has been considered. This is an idealization that obviously does not reflect the reality, but it was considered an appropriate simplification for the case that was being studied. However, it would not be the case when analysing the holding capacity, where a model of the soil and its interaction with the suction skirts shall be performed.

8.3 Conclusions

In this research project, the study of different design cases of the Ocean Grazer suction caisson have been performed, by means of finite elements analysis and backed by theoretical calculations, with the scope of delivering design guidelines that can be trustfully used and considered in following stages of the design process. A summery of these guidelines is depicted:

- Information about the type of soil and its properties is essential to know how to proceed in the calculations of the system's boundary conditions.
- A rectangular-shape suction caisson with similar dimensions to those required by the Ocean Grazer will necessarily need some kind of reinforcement that provides stiffness and resistance to the structure.
- When installing the suction caisson in uniform sand, several considerations can be done:
  - Installation in loose seabeds, compartmentalization of the suction caisson, or increase of the reinforcement spacing will have an effect on the design, making it lighter and therefore cheaper to build, but still resistant enough to meet the solicitations.
  - If more than one of the variables expressed in the previous paragraph are modified, interactions between them must be taken into account. An increase in the beam spacing or the research of a location with looser sand will have a great impact only when the number of compartments in which the suction caisson is divided is low.
- It has been proved that a larger effective force of the structure has a great effect on the installation of the caisson, decreasing the extreme solicitations acting on the structure. Therefore, procedures to increase this force during the installation process (mainly by means of using temporal extra weight) could minimize the necessity of over-sizing a structure with a large amount of reinforcement, only designed with the aim of making possible its installation. In that case, and with accordance to the proposed further research, other stages of the suction caisson lifetime should be studied, specially its extraction for maintenance.
- The connections between structural elements such as beams and columns need special attention. The concentration of stresses that normally occur in these areas implies the introduction of elements such as stiffeners or haunches. The latter is specially interesting for long spans as this case. A 10-15% length and height is recommended.

References

ABS (2016). *Guide for load and resistance factor design (LRFD) criteria for offshore structures.* American Bureau of Shipping.

Arany, L. and Bhattacharya, S. (2018). Simplified load estimation and sizing of suction anchors for spar buoy type floating offshore wind turbines. (English). *Ocean Engineering*, 159.

Bhattacharya, S., Nikitas, G., Arany, L., and Nikitas, N. (2017). Soil-structure interactions (ssi) for offshore wind turbines. *IET Reference*, 1.

Cathie, D. and Irvine, J. (2019). Suction installed caisson foundations for offshore wind: Design guidelines.

CEN (2005). *EN 1993-1-1. Eurocode 3: Design of Steel Structures-part 1-1: General rules and rules for buildings.* European Committee for Standardization - Comité Européen de Normalisation.

Chatzivasileiou, I. G. (2014). Installation of suction caissons in layered sand. assessment of geotechnical aspects.

DNV-GL (2016). *Design of offshore steel structures, general - LRFD method.* Det Norske Veritas and Germanischer Lloyd.

Guo, W. and Chu, J. (2014). Suction caisson installation in shallow water: Model tests and prediction.

Houlsby, G. and Byrne, B. (2005). Design procedures for installation of suction caissons in sand. *Proceedings of The Institution of Civil Engineers-geotechnical Engineering - PROC INST CIVIL ENG-GEOTECH E*, 158:135–144.

Houlsby, G., Kelly, R., and Byrne, B. (2005). The tensile capacity of suction caissons in sand under rapid loading.

Ibsen, L. and Thilsted, C. (2010). Numerical study of piping limits for suction installation of offshore skirted foundations and anchors in layered sand.

Lindeburg, M. R. (1999). *Civil Engineering Reference Manual for the PE Exam.* Professional Publications, Belmont, CA.

Netherlands Enterprise Agency (2016). Geotechnical Report/Investigation Data. Seafloor In Situ Test Locations. Borssele Wind Farm Site IV.

Pollestad, J. (2015). Investigation of suction anchor pullout capacity under undrained conditions.

Tassoulas, J., Maniar, D., and Vásquez, L. (2005). Suction caissons: Finite element modeling.

Tjelta, T. (2015). The suction foundation technology. *Frontiers in Offshore Geotechnics III.*

UCLM (2005). Tema 3: Tipologia de uniones entre elementos estructurales.

Appendices

A Appendix. Suction caissons calculations literature

Appendix content

Appendix A synthesizes information found in literature which is used and accordingly referenced throughout the thesis. The first two sections depict basic theory, aiming to provide context for the methods later exposed. As discussed in section 6.3, different calculation methods have been largely studied and used in recent years. The author of this paper has not carried out exhaustive research or compared their performance in order to decide the convenience of using one or another. On the contrary, according to the conclusions found in previous research papers, a method has been chosen in each case.

A.1 Soil vertical stress

The vertical stress on a point within the soil, due to self weight, increase with depth and can be determined from the mass of the overlying material. If γ is the unit weight of the soil and y is a certain depth, the vertical stress at that point is $\sigma_y = \gamma y$.
When the soil is under water, the weight of all materials, solid and water, is accounted to calculate the total vertical stress at depth y ($y = 0$ at soil surface) as follows: $\sigma_{y,total} = \gamma_w y_w + \gamma_{sat} y$, where y_w is the water depth above soil, γ_w is the water unit weight, γ_{sat} is the saturated unit weight of soil, which is the unit weight of a soil when all void spaces of the soil are completely filled with water.
In the case of the pores of a soil mass being filled with water, if a pressure is induced into the pore water, a force appears trying to separate the grains, which is known as the pore water pressure: $u_y = \gamma_w(y_w + y)$.
The difference between the total stress and the pore pressure in a saturated soil has been defined as the effective stress: $\sigma_y^{'} = \sigma_{y,total} - u_y = (\gamma_{sat} - \gamma_w)y = \gamma^{'} y$, where $\gamma^{'}$ is known as the effective unit weight of soil.

A.2 Conventional pile design calculations

In order to calculate the friction vertical forces that soil apply against a certain area, such as the skirt of a suction caisson, this theoretical background is widely used. In the case of conventional pile design practice, an average stress acting on the whole skirt length is accounted for $\gamma^{'}\frac{y}{2}$. A K parameter is also used as a factor relating vertical stress to horizontal stress. This horizontal stress acts on the whole skirt area, calculated as Py, where P is the perimeter of the wall and y is the penetrated depth. A δ parameter is also used, known as the angle of interface friction between the soil and the skirt, and it is always related to the beforehand mentioned K parameter. Hence, the vertical friction on a wall can be calculated as:

$$Q = \frac{\gamma^{'} y^2}{2}(K \tan\delta)P$$

Therefore, the result for the vertical load on the caisson for penetration to depth h, in the absence of suction, is given by:

$$V^{'} = \frac{\gamma^{'} h^2}{2}(K \tan\delta)_o P_o + \frac{\gamma^{'} h^2}{2}(K \tan\delta)_i P_i + \left(\gamma^{'} h N_q + \gamma^{'}\frac{t}{2}N_\gamma\right) A_{tip} \tag{31}$$

where the first term accounts for the friction on the outside of the skirt, the second for the friction on the inside and the third for the end bearing on the annulus (Houlsby and Byrne (2005)).

If the inwards movement of soil due to suction is not taken into account, the factor sA_i can be added at the left term of the equation, so that the suction needed can be calculated.

A.3 Holding capacity of suction caissons in sand

Houlsby et al. (2005), in a study about the tensile capacity of suction caissons in sand, conclude that it is unconservative to ignore the reduction of vertical stress within the soil close to the caisson due to the frictional forces along the caisson skirt. That is why they develop a theory which takes

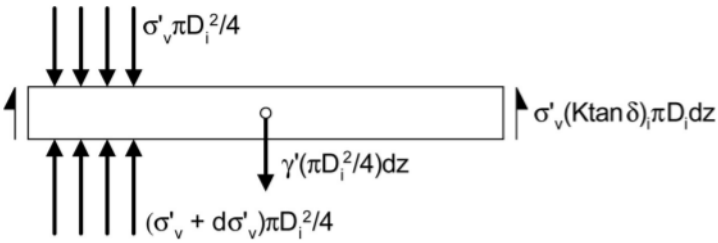

Figure 63: *Equilibrium of slice of soil within caisson when pulling it up (Houlsby et al. (2005))*

this into account, as resumed in the following paragraphs.

Firstly, they consider the soil within the internal walls of the caisson. Assuming that the vertical effective stress is constant across the section of the caisson and taking into account the forces applied on a disk of soil (see Figure 63), the vertical equilibrium equation is as follows:

$$\sigma_v^{'} A_i - (\sigma_v^{'} + d\sigma_v^{'}) A_i - \sigma_v^{'} (K \tan\delta)_i P_i dz + \gamma^{'} A_i dz = 0 \tag{32}$$

which can be rewritten as

$$\frac{d\sigma_v^{'}}{dz} = \gamma^{'} - \frac{\sigma_v^{'} (K \tan\delta)_i P_i}{A_i}$$

This equation becomes

$$\frac{d\sigma_v^{'}}{dz} = \gamma^{'} - \frac{\sigma_v^{'}}{Z_i} \tag{33}$$

where

$$Z_i = \frac{A_i}{(K \tan\delta)_i P_i} \tag{34}$$

The solution of equation 33 is

$$\sigma_v^{'} = \gamma^{'} Z_i (1 - exp\left(-\frac{z}{Z_i}\right)) \tag{35}$$

which gives the effective vertical stress at a certain depth; for instance, at z=0, $\sigma_v^{'} = 0$. However, the total friction force depends on the integral along the penetrated length of the skirt, as follows

$$\int_0^h \sigma_v^{'} dz = \gamma^{'} Z_i^2 (exp\left(-\frac{h}{Z_i}\right) - 1 + \left(\frac{h}{Z_i}\right)) \tag{36}$$

A similar analysis can be done for the sand outside the caisson, with equations 35 and 41 being the same but changing Z_i for Z_o, which can be calculated as

$$Z_o = \frac{A_m - A_o}{(K \tan\delta)_o P_o} \tag{37}$$

A_m is the area of the boundary within the enhancement of the stress is considered. Its formulation is for a cylindrical case, so that the diameter D_m is defined as $D_m = mD_o$, where m is a multiple of the outer diameter of the caisson. D_o and D_m comprise the region where the vertical stress is reduced. In this case, where a square-shape caisson is considered, the same relation is defined for the length and width of the caisson ($l_m = ml_o$ and $w_m = mw_o$). It is wise to think that the sharp corners of the caisson will have an effect on this parameter m, probably reducing the friction occurring. No formulation will be applied approaching this phenomena, but it should be kept in mind; while it is conservative when installing the caisson, it happens to be the opposite situation in the holding capacity calculation.

Hence, the friction forces inside and outside the caisson can be calculated as follows, using ecuation 41:

$$Q_{out} = \int_0^h \sigma_{vo}^{'} dz (K \tan\delta)_o P_o \tag{38}$$

$$Q_{in} = \int_0^h \sigma_{vi}^{'} dz (K \tan\delta)_i P_i \tag{39}$$

Therefore, the vertical capacity in sand accounting for the effects of enhancement can be calculated as (the ocean pressure is not taken into account, but it is a conservative approach):

$$V_{c,sand} = W_{rt} + W_{sc} + Q_{out} + Q_{in} \tag{40}$$

$V_{c,sand}$	vertical capacity in sand	(kN)
W_{rt}	Concrete rigid tank weight	(kN)
W_{sc}	Steel suction caisson weight	(kN)
Q_{in}	Friction forces inside the caisson	(kN)
Q_{out}	Friction forces outside the caisson	(kN)

Equation 40 can therefore be expressed as:

$$\begin{aligned} V_{c,sand} = \quad & W_{rt} + W_{sc} \\ & + \gamma^{'} Z_o^2 \left(exp\left(-\frac{h}{Z_o}\right) - 1 + \left(\frac{h}{Z_o}\right)\right) (K \tan\delta)_o P_o \\ & + \gamma^{'} Z_i^2 \left(exp\left(-\frac{h}{Z_i}\right) - 1 + \left(\frac{h}{Z_i}\right)\right) (K \tan\delta)_i P_i \end{aligned}$$

A.4 Suction caisson installation in sand calculations

The same authors (Houlsby and Byrne (2005)), in another document about design procedures for installation of suction caissons, present a similar procedure. As shown in figure 64, the equilibrium of forces within a piece of soil is again considered, with the slight difference of the outer friction having the opposite direction.

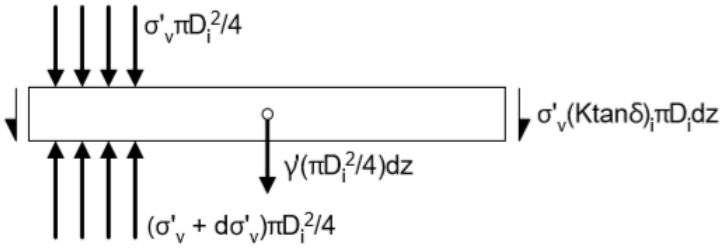

Figure 64: *Equilibrium of slice of soil within caisson during installation (Houlsby and Byrne (2005))*

Analogous to the previous section, the equilibrium of forces leads to the following equation:

$$\int_0^h \sigma_v^{'} dz = \gamma^{'} Z_i^2 \left(exp\left(\frac{h}{Z_i}\right) - 1 - \left(\frac{h}{Z_i}\right)\right) \tag{41}$$

A part form the friction on the inside and outside of the caisson, an end bearing term is also accounted for. Its calculation and the final expressions for the two-phases suction caisson installation procedure are presented in section 6.3.

A.5 Bearing capacity factors

The N_q and N_γ factors are known as bearing capacity factors, widely used in foundation calculations. There are several formulations to calculate them, which lead to similar results. The ones used in this paper are the following:

- N_q is derived from the Prandtl-Reissner expression:

$$N_q = e^{\pi \tan\phi} \tan^2(45^\circ + \frac{\phi}{2}) \tag{42}$$

- N_γ is calculated with Meyerhof (1963) expression:

$$N_\gamma = (N_q - 1)\tan(1,4\phi) \tag{43}$$

A.6 Soil properties. Sand

All the calculation procedures found in literature distinguish between two cases (sand and clay), leading to distinct formulations.
The seabed content depends mainly on the location. While a difference between clay and sand can be made, most locations show a layered soil profile, where layers of these two types of soil with different properties are present. However, it has been found that, in many cases, the first layers of soil are made of loose to dense sand. For example, in a study made by the Dutch government in different location within the North Sea, at least the first 10m depth always contained sand of different types (Netherlands Enterprise Agency (2016)).

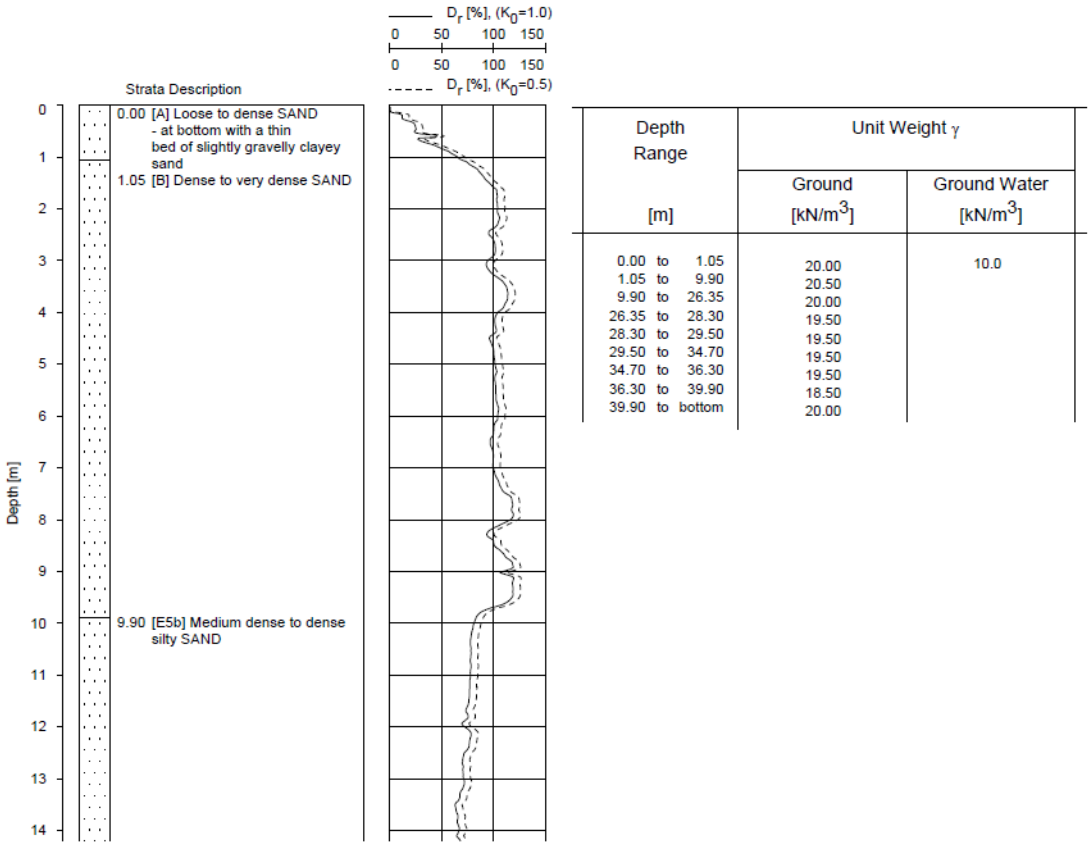

Depth Range [m]	Unit Weight γ Ground [kN/m^3]	Unit Weight γ Ground Water [kN/m^3]
0.00 to 1.05	20.00	10.0
1.05 to 9.90	20.50	
9.90 to 26.35	20.00	
26.35 to 28.30	19.50	
28.30 to 29.50	19.50	
29.50 to 34.70	19.50	
34.70 to 36.30	19.50	
36.30 to 39.90	18.50	
39.90 to bottom	20.00	

Figure 65: *Relative density and effective unit weight. Test CPT.WFS4.28 (Netherlands Enterprise Agency (2016))*

Depending on the calculation method used for suction caissons, different soil parameters can be needed. In the following paragraphs, the sand properties relevant to this thesis will be discussed. Most of these parameters have been defined in previous sections of this annex.

- Effective unit weight of soil ($\gamma^{'}$), calculated as the submerged unit weight of the soil (γ_{sat}) minus the unit weight of water ($\gamma_w = 9,81 kN/m^3$). Netherlands Enterprise Agency (2016) found the submerged unit weight of soil in all locations tested had values ranging from 18 to 20 kN/m^3. Similar values can be found in other publications, where classifications from loose to dense sand show γ_{sat} between 18,5 and 20,4 kN/m^3 respectively (Lindeburg (1999)).
- Angle of internal friction of the soil (ϕ). Literature shows that the internal friction of sand goes from 30 to 45°.

Table 14: *Relationship between Relative Density (D_r) and Angle of Internal Friction (ϕ) in sand (Lindeburg (1999))*

Type of soil	Angle of internal friction, (°) Meyerhof 1956	Relative density, D_r (%)
very loose sand	<30	<20
loose sand	30-35	20-40
medium sand	35-40	40-60
dense sand	40-45	60-80
very dense sand	>45	>80

As it can be seen from this table, another parameter related to the angle of internal friction is the relative density, also depicted in figure 65. The same source define the relative density as *the ratio of the difference between the void ratios of a cohesionless soil in its loosest state and existing natural state to the difference between its void ratio in the loosest and densest states.*

- Interface friction angle (δ), also known as the external or wall friction angle, is the angle between the normal of a wall and the direction of the resultant pressure that the soil exerts on that wall. It can be estimated as $\frac{1}{3}\phi$ for smooth retaining walls, or $\frac{2}{3}\phi$ for rougher surfaces. Values of this angle can be found tabulated for a variety of interface materials. For instance, a steel sheet pile against sand ranges from 11° to 14°.

- Factor relating vertical stress to horizontal stress (K), also known as the lateral earth pressure coefficient for soils, it is widely used for retaining walls. Earth pressure is the force per unit area exerted by soil on the retaining wall. Different formulations have been proposed to calculate what it is known as the active earth pressure, the passive earth pressure or the at-rest soil pressure. There are three main earth pressure theories: the Rankine theory, the Coulomb theory and the log-spiral theory.
  The active earth pressure is present behind a retaining wall that moves away from and tensions the remaining soil. A simplified formulation where the backfill is horizontal, the wall face is vertical and the friction between the wall and the soil is disregarded ($\delta = 0$) is:

$$k_a = \frac{1}{k_p} = \tan^2(45^o - \frac{\phi}{2}) = \frac{1 - \sin(\phi)}{1 + \sin(\phi)}$$

  The passive earth pressure is present inf front of a retaining wall that moves toward and compresses the soil. Equally, an ecuation can be formulated as:

$$k_a = \frac{1}{k_a} = \tan^2(45^o + \frac{\phi}{2}) = \frac{1 + \sin(\phi)}{1 - \sin(\phi)}$$

  In some cases, the soil is completely confined and the walls do not move, situations known as "at rest" earth pressure, which can be expressed as:

$$k_o \approx 1 - \sin(\phi)$$

- Ratio of permeability within caisson to outside caisson (k_f), calculated as the fraction between the permeability of the soil inside the caisson and outside the caisson ($k_f = k_i/k_o$). This ratio will affect the value of the parameter a, which can be obtained as shown in section 6.3.2. Depending on the soil and the interaction of this with the structure, different values can be used, starting at 1 and up to 5 (Houlsby and Byrne (2005)).

B Appendix. Factorial design runs

Appendix content
Appendix B includes all the data calculated when carrying out the factorial design, the results of which are analysed in section 7.4

B.1 Run 1

Table 15: *Factor values used in run 1*

A	B	C
Sand properties	Number of compartments	Reinforcement spacing
Loose sand $\gamma' = 8.19kN/m^3$ Ktan $\delta = 0.5$ $\phi = 30^o$	1	0,5

Preliminary stage
An initial value of $V' = 3000kN$ is set. Using equations 26 and 27, the self-weight penetration depth and suction needed are calculated: $h_{sw} = 2.4m; s = 77.26kPa$.

The magnifying factor (1.5) as well as the width of the structure that accounts for each frame (the reinforcement spacing. Factor C), will be applied to find the suction that should be considered: $s = 77.26 * 1.5 * 0.5 = 57.95kPa$.

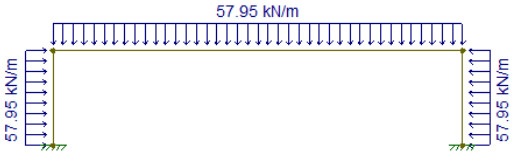

Figure 66: *Loading diagram run 1, preliminary stage*

The Cross method (using F-tools software) is applied in order to find the bending and normal forces diagrams. In this case, since the profile is still indeterminate, all bars have the same inertia.
As it can be seen in the following figures, the maximum values in each case are:

Beam: M=1725 kNm
Pillars: M=1725 kNm

Beam: N=643.5 kN
Pillars: N=579.5 kN

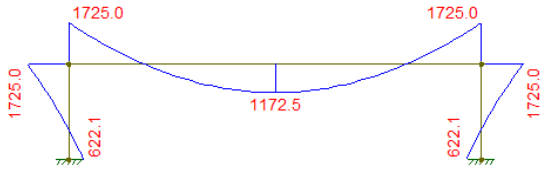

Figure 67: *Bending stress diagram run 1, preliminary stage*

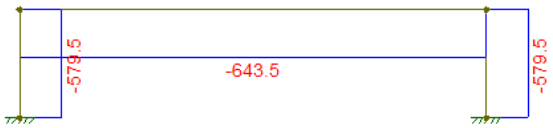

Figure 68: *Normal stress diagram run 1, preliminary stage*

Different profiles are set for both the beam and pillars. Using equation 28, the profiles can be verified, calculating the percentage of the structure utilization (which can also be though as the coefficient of security).

- Beam: HE 650 B. 98%
- Pillars: HE 550 B. 98%

1st iteration
With these profiles, the volume of the whole structure is calculated. Volume=$58.12m^3$, which leads

to a recalculated $V^{'} = 3894kN$. The self-weight penetration depth and suction needed are now: $h_{sw} = 2.78m; s = 79.44kPa$, which after applying the factors, $s = 59.58kPa$.
Again, the Cross method is used to obtained the following diagrams:

Beam: M=1704.4 kNm
Pillars: M=1704.4 kNm

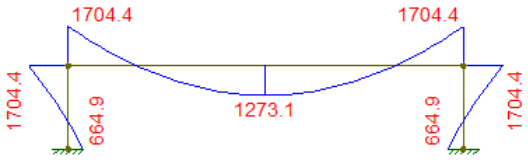

Figure 69: *Bending stress diagram run 1, 1st iteration*

Beam: N=688.1 kN
Pillars: N=595.5 kN

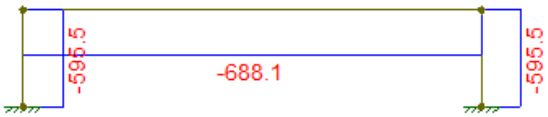

Figure 70: *Normal stress diagram run 1, 1st iteration*

Now, the validation of the profiles is recalculated:

- Beam: HE 650 B. 99%
- Pillars: HE 550 B. 99%

B.2 Run 2

Table 16: *Factor values used in run 2*

A	B	C
Sand properties	Number of compartments	Reinforcement spacing
Dense sand $\gamma^{'} = 10.19kN/m^3$ Ktan $\delta = 0.8$ $\phi = 45^o$	1	0,5

Preliminary stage
Initial value of $V^{'} = 4000kN \rightarrow h_{sw} = 0.92m; s = 144.44kPa \rightarrow s = 144.44{*}1.5{*}0.5 = 108.33kPa$.

Beam: M=3157.9 kNm
Pillars: M=3157.9 kNm

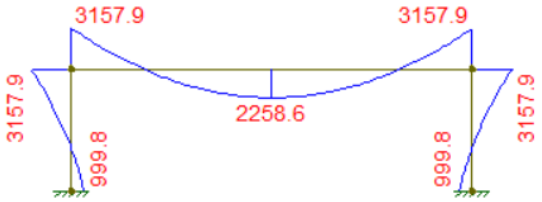

Figure 71: *Bending stress diagram run 2, preliminary stage*

Beam: N=1013.2 kN
Pillars: N=1083.3 kN

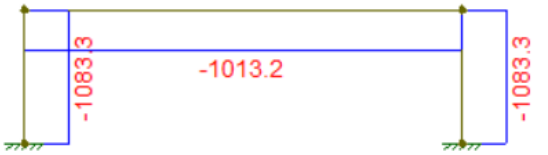

Figure 72: *Normal stress diagram run 2, preliminary stage*

- Beam: HE 1000 B. 100%
- Pillars: HE 900 B. 85%

1st iteration
Volume=$73.61m^3 \rightarrow V^{'} = 4932kN$.
$h_{sw} = 1.1m; s = 144.92kPa \rightarrow s = 108.69kPa$.

Beam: M=3054.5 kNm
Pillars: M=3054.5 kNm

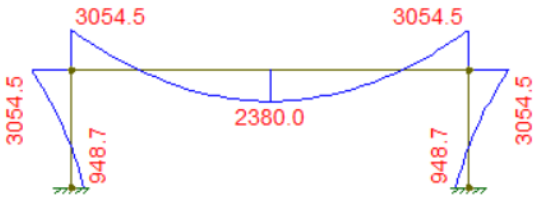

Figure 73: *Bending stress diagram run 2, 1st iteration*

Beam: N=999.1 kN
Pillars: N=1086.9 kN

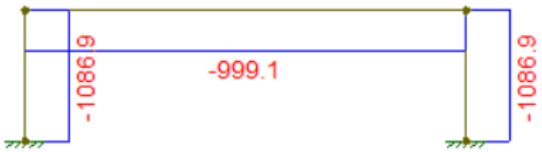

Figure 74: *Normal stress diagram run 2, 1st iteration*

- Beam: HE 1000 B. 97%
- Pillars: HE 900 B. 82%

B.3 Run 3

Table 17: *Factor values used in run 3*

A	B	C
Sand properties	Number of compartments	Reinforcement spacing
Loose sand $\gamma^{'} = 8.19kN/m^3$ Ktan $\delta = 0.5$ $\phi = 30^o$	5	0,5

Preliminary stage
Initial value of $V^{'} = 3000kN$.
$h_{sw} = 1.7m; s = 101.13kPa \rightarrow s = 101.13 * 1.5 * 0.5 = 75.85kPa$.

Central beams: M=107.8 kNm
Outer beams: M=133.2 kNm
Pillars: M=227.0 kNm

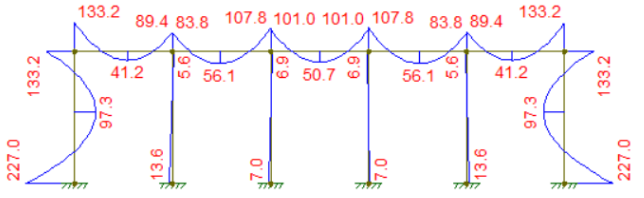

Figure 75: *Bending stress diagram run 3, preliminary stage*

Central beams: N=183.5 kN
Outer beams: N=187.0 kN
Pillars: N=162.7 kN

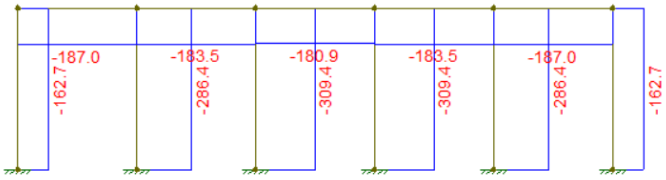

Figure 76: *Normal stress diagram run 3, preliminary stage*

- Central beams: HE 160 B. 103%
- Outer beams: HE 180 B. 92%
- Pillars: HE 220 B. 88%

1st iteration
Volume=$53.28m^3 \rightarrow V^{'} = 3570kN$
$h_{sw} = 1.87m; s = 103.12kPa \rightarrow s = 77.34kPa.$

Central beams: M=104 kNm
Outer beams: M=123.7 kNm
Pillars: M=195.5 kNm

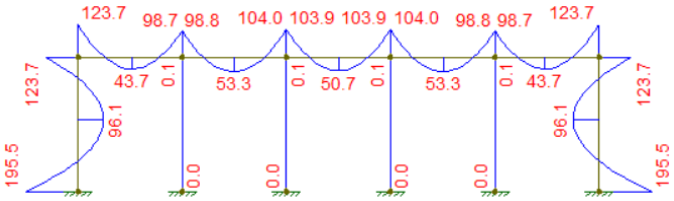

Figure 77: *Bending stress diagram run 3, 1st iteration*

Central beams: N=184.4 kN
Outer beams: N=184.4 kN
Pillars: N=160.9 kN

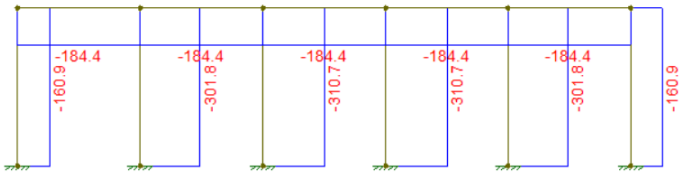

Figure 78: *Normal stress diagram run 3, 1st iteration*

- Central beams: HE 160 B. 100%
- Outer beams: HE 180 B. 86%
- Pillars: HE 220 B. 77%

B.4 Run 4

Table 18: *Factor values used in run 4*

A	B	C
Sand properties	Number of compartments	Reinforcement spacing
Dense sand $\gamma^{'} = 10.19kN/m^3$ Ktan $\delta = 0.8$ $\phi = 45^o$	5	0,5

Preliminary stage
Initial value of $V^{'} = 3000kN$.
$h_{sw} = 0.6m; s = 147.8kPa \rightarrow s = 147.8 * 1.5 * 0.5 = 110.85kPa$.

Central beams: M=157.5 kNm
Outer beams: M=269 kNm
Pillars: M=466.1 kNm

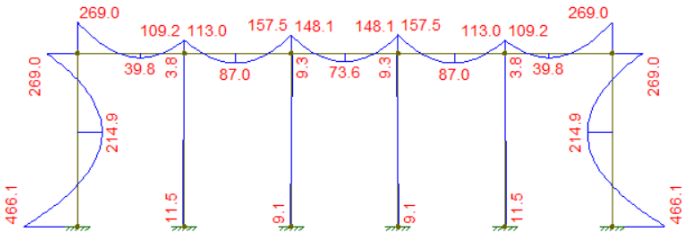

Figure 79: *Bending stress diagram run 4, preliminary stage*

Central beams: N=326.4 kN
Outer beams: N=327.5 kN
Pillars: N=261.7 kN

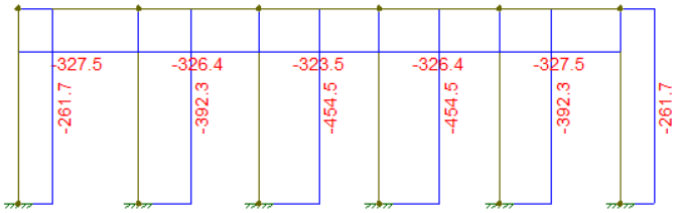

Figure 80: *Normal stress diagram run 4, preliminary stage*

- Central beams: HE 200 B. 87%
- Outer beams: HE 220 B. 109%
- Pillars: HE 280 B. 97%

1st iteration
Volume=$57.54m^3 \rightarrow V^{'} = 3855kN$
$h_{sw} = 0.74m; s = 147.72kPa \rightarrow s = 110.79kPa$.

Central beams: M=151 kNm
Outer beams: M=221.1 kNm
Pillars: M=437.7 kNm

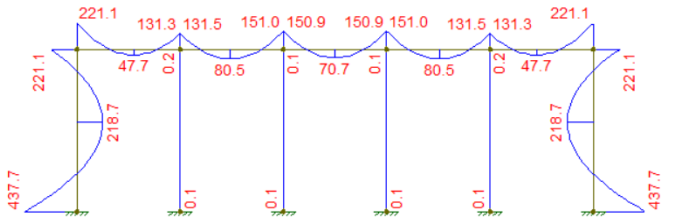

Figure 81: *Bending stress diagram run 4, 1st iteration*

Central beams: N=312.2 kN
Outer beams: N=312.2 kN
Pillars: N=244 kN

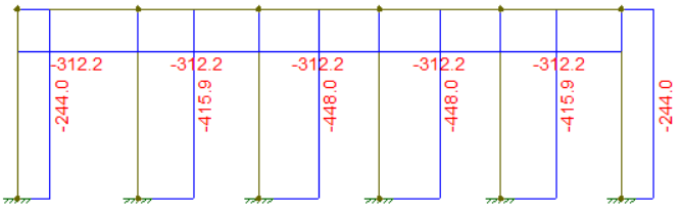

Figure 82: *Normal stress diagram run 4, 1st iteration*

- Central beams: HE 200 B. 84%

- Outer beams: HE 220 B. 91%
- Pillars: HE 280 B. 91%

B.5 Run 5

Table 19: *Factor values used in run 5*

A	B	C
Sand properties	Number of compartments	Reinforcement spacing
Loose sand $\gamma^{'} = 8.19kN/m^3$ Ktan $\delta = 0.5$ $\phi = 30^o$	1	1

Preliminary stage
Initial value of $V^{'} = 3000kN$.
$h_{sw} = 2.4m; s = 68.18kPa$.
$s = 68.18 * 1.5 * 1 = 102.27kPa$.

Beam: M=3044.3 kNm
Pillars: M=3044.3 kNm

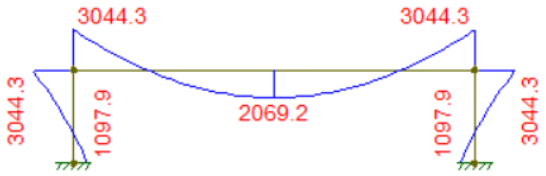

Figure 83: *Bending stress diagram run 5, preliminary stage*

Beam: N=1135.7 kN
Pillars: N=1022.7 kN

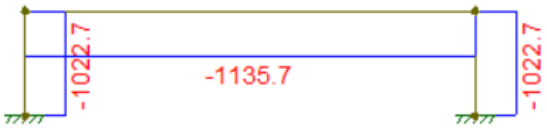

Figure 84: *Normal stress diagram run 5, preliminary stage*

- Beam: HE 1000 B. 100%
- Pillars: HE 800 B. 98%

1st iteration
Volume=$48.04m^3 \rightarrow V^{'} = 3219kN$.
$h_{sw} = 2.5m; s = 69.62kPa \rightarrow s = 104.43kPa$.

Beam: M=2875.3 kNm
Pillars: M=2875.3 kNm

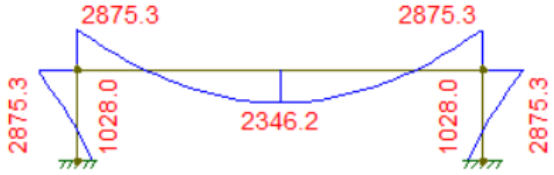

Figure 85: *Bending stress diagram run 5, 1st iteration*

Beam: N=1102.4 kN
Pillars: N=1044.3 kN

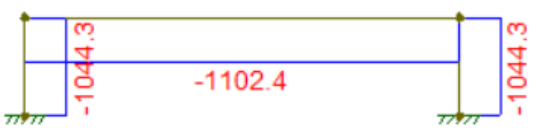

Figure 86: *Normal stress diagram run 5, 1st iteration*

- Beam: HE 1000 B. 98%
- Pillars: HE 800 B. 93%

B.6 Run 6

Table 20: *Factor values used in run 6*

A	B	C
Sand properties	Number of compartments	Reinforcement spacing
Dense sand $\gamma^{'} = 10.19kN/m^3$ Ktan $\delta = 0.8$ $\phi = 45^o$	1	1

Preliminary stage
Initial value of $V^{'} = 4000kN$.
$h_{sw} = 0.92m; s = 140.48kPa$.
$s = 140.48 * 1.5 * 1 = 210.72kPa$.

Beam: M=6142.6 kNm
Pillars: M=6142.6 kNm

Beam: N=1970.8 kN
Pillars: N=2107.2 kN

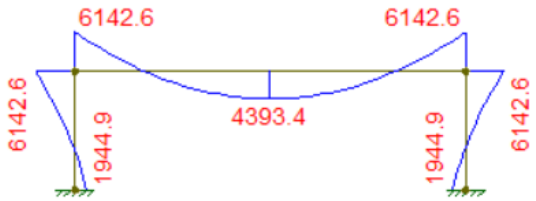

Figure 87: *Bending stress diagram run 6, preliminary stage*

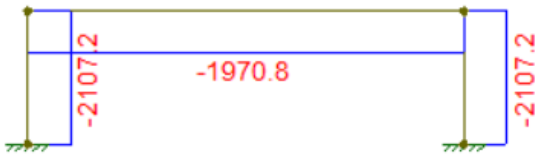

Figure 88: *Normal stress diagram run 6, preliminary stage*

- Beam: HL 920 x 534. 96%
- Pillars: HL 920 x 446. 100%

1st iteration
Volume=$64.87m^3 \rightarrow V^{'} = 4346kN$.
$h_{sw} = 0.99m; s = 140.50kPa \rightarrow s = 210.75kPa$.

Beam: M=6092.2 kNm
Pillars: M=6092.2 kNm

Beam: N=1955.8 kN
Pillars: N=2107.5 kN

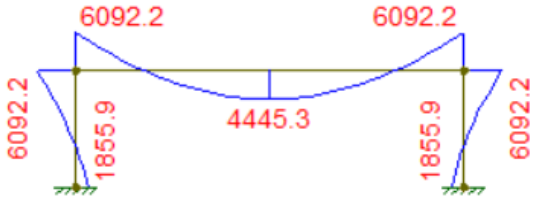

Figure 89: *Bending stress diagram run 6, 1st iteration*

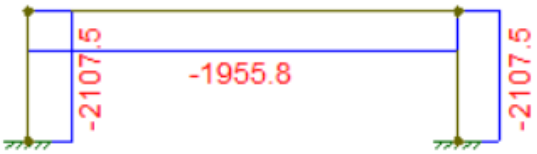

Figure 90: *Normal stress diagram run 6, 1st iteration*

- Beam: HL 920 x 534. 95%
- Pillars: HL 920 x 446. 100%

B.7 Run 7

Table 21: *Factor values used in run 7*

A	B	C
Sand properties	Number of compartments	Reinforcement spacing
Loose sand $\gamma^{'} = 8.19kN/m^3$ Ktan $\delta = 0.5$ $\phi = 30^o$	5	1

Preliminary stage
Initial value of $V^{'} = 3000kN$.
$h_{sw} = 1.71m; s = 92.84kPa \rightarrow s = 92.84 * 1.5 * 1 = 139.26kPa$.

Central beams: M=198 kNm
Outer beams: M=237 kNm
Pillars: M=402.6 kNm

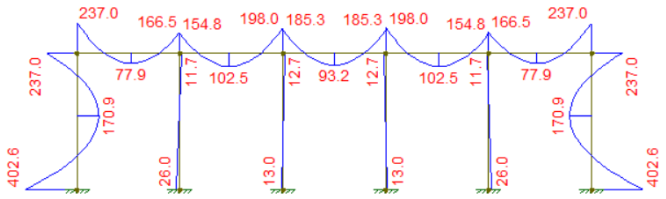

Figure 91: *Bending stress diagram run 7, preliminary stage*

Central beams: N=329.9 kN
Outer beams: N=337 kN
Pillars: N=296.2 kN

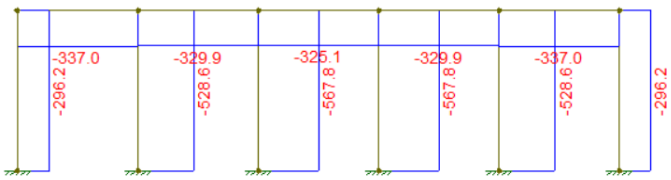

Figure 92: *Normal stress diagram run 7, preliminary stage*

- Central beams: HE 200 B. 106%
- Outer beams: HE 220 B. 98%
- Pillars: HE 260 B. 102%

1st iteration
Volume=$50.64m^3 \rightarrow V^{'} = 3393kN$
$h_{sw} = 1.82m; s = 92.49kPa \rightarrow s = 138.74kPa.$

Central beams: M=186.9 kNm
Outer beams: M=227.5 kNm
Pillars: M=358.3 kNm

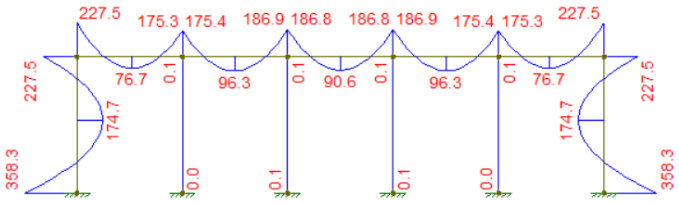

Figure 93: *Bending stress diagram run 7, 1st iteration*

Central beams: N=334.1 kN
Outer beams: N=334.1 kN
Pillars: N=290.5 kN

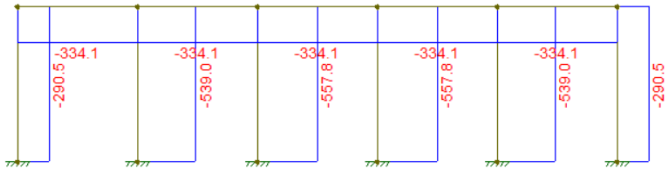

Figure 94: *Normal stress diagram run 7, 1st iteration*

- Central beams: HE 200 B. 100%
- Outer beams: HE 220 B. 94%
- Pillars: HE 260 B. 91%

B.8 Run 8

Table 22: *Factor values used in run 8*

A	B	C
Sand properties	Number of compartments	Reinforcement spacing
Dense sand $\gamma^{'} = 10.19kN/m^3$ Ktan $\delta = 0.8$ $\phi = 45^o$	5	1

Preliminary stage
Initial value of $V^{'} = 3000kN$.
$h_{sw} = 0.6m; s = 146.59kPa \rightarrow s = 146.59 * 1.5 * 1 = 219.89kPa.$

Central beams: M=312.4 kNm
Outer beams: M=524.4 kNm
Pillars: M=908.4 kNm

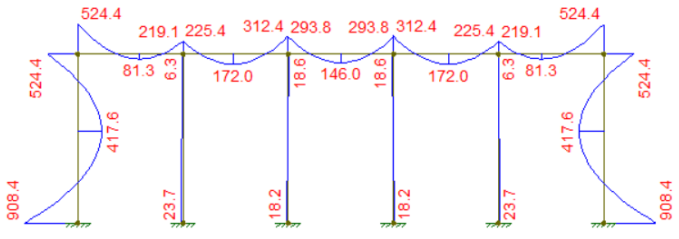

Figure 95: *Bending stress diagram run 8, preliminary stage*

Central beams: N=640.9 kN
Outer beams: N=524.4 kN
Pillars: N=908.4 kN

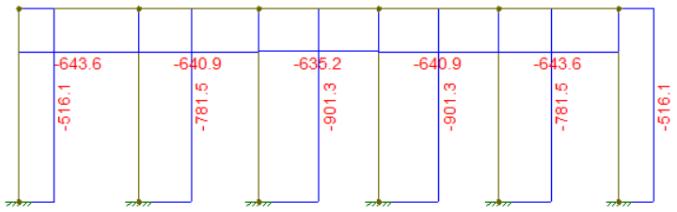

Figure 96: *Normal stress diagram run 8, preliminary stage*

- Central beams: HE 260 B. 90%
- Outer beams: HE 300 B. 97%
- Pillars: HE 400 B. 92%

1st iteration
Volume=$54.56m^3 \rightarrow V^{'} = 3656kN$
$h_{sw} = 0.71m; s = 146.51kPa \rightarrow s = 219.77kPa.$

Central beams: M=299.2 kNm
Outer beams: M=440.8 kNm
Pillars: M=887.7 kNm

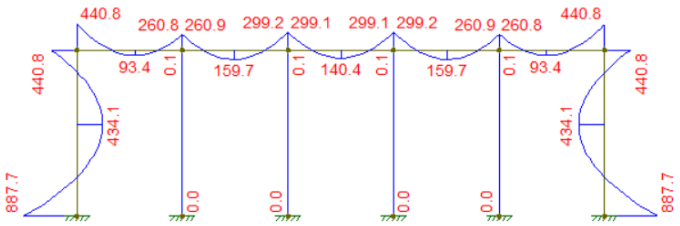

Figure 97: *Bending stress diagram run 8, 1st iteration*

Central beams: N=620.2 kN
Outer beams: N=620.1 kN
Pillars: N=484.5 kN

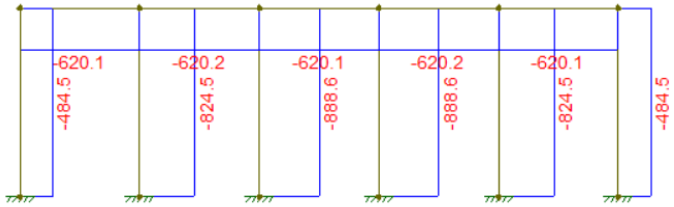

Figure 98: *Normal stress diagram run 8, 1st iteration*

- Central beams: HE 260 B. 83%
- Outer beams: HE 280 B. 100%
- Pillars: HE 400 B. 90%